BOUNDARY LAYER STUDIES ON A SPINNING CONE

Walter B. Sturek

Ballistic Research Laboratories
Aberdeen Proving Ground, Maryland

May 1973

BRL R 1649

BRL

AD

REPORT NO. 1649

BOUNDARY LAYER STUDIES ON A SPINNING CONE

by

Walter B. Sturek

May 1973

USA BALLISTIC RESEARCH LABORATORIES
ABERDEEN PROVING GROUND, MARYLAND

46

Destroy this report when it is no longer needed.
Do not return it to the originator.

Secondary distribution of this report by originating or sponsoring activity is prohibited.

Additional copies of this report may be obtained from the National Technical Information Service, U.S. Department of Commerce, Springfield, Virginia 22151.

The findings in this report are not to be construed as an official Department of the Army position, unless so designated by other authorized documents.

UNCLASSIFIED
Security Classification

DOCUMENT CONTROL DATA - R & D

(Security classification of title, body of abstract and indexing annotation must be entered when the overall report is classified)

1. ORIGINATING ACTIVITY (Corporate author) US Army Ballistic Research Laboratories Aberdeen Proving Ground, Maryland 21005	2a. REPORT SECURITY CLASSIFICATION UNCLASSIFIED 2b. GROUP

3. REPORT TITLE

BOUNDARY LAYER STUDIES ON A SPINNING CONE

4. DESCRIPTIVE NOTES (Type of report and inclusive dates)

5. AUTHOR(S) (First name, middle initial, last name)

Walter B. Sturek

6. REPORT DATE	7a. TOTAL NO. OF PAGES	7b. NO. OF REFS
MAY 1973	51	7

8a. CONTRACT OR GRANT NO. b. PROJECT NO. RDT&E Project No. 1T061102A33D c. d.	9a. ORIGINATOR'S REPORT NUMBER(S) BRL Report No. 1649 9b. OTHER REPORT NO(S) (Any other numbers that may be assigned this report)

10. DISTRIBUTION STATEMENT

Approved for public release; distribution unlimited.

11. SUPPLEMENTARY NOTES	12. SPONSORING MILITARY ACTIVITY
	US Army Materiel Command Washington, D. C.

13. ABSTRACT

An experimental investigation of the effects of spin induced distortion of the boundary layer on a spinning 10° half angle cone at Mach 2, 3 and 4 is reported. The profile of the location of boundary layer transition has been determined completely about the surface of the cone model from spark shadowgraphs. These spark shadowgraphs were taken with the model mounted on an offset strut which was rolled incrementally in azimuth to reveal the entire surface of the model. The profile of the boundary layer thickness at the base of the cone has also been determined from the spark shadowgraphs. Strain gage balance measurements of Magnus and normal force were made for three significantly different boundary layer configurations and confirm the extreme sensitivity of Magnus to boundary layer configuration.

DD FORM 1 NOV 68 1473 REPLACES DD FORM 1473, 1 JAN 64, WHICH IS OBSOLETE FOR ARMY USE.

UNCLASSIFIED
Security Classification

14. KEY WORDS	LINK A		LINK B		LINK C	
	ROLE	WT	ROLE	WT	ROLE	WT
Boundary Layer Transition Magnus Force Measurements Asymmetric Bodies Three-Dimensional Boundary Layer						

BALLISTIC RESEARCH LABORATORIES

REPORT NO. 1649

MAY 1973

BOUNDARY LAYER STUDIES ON A SPINNING CONE

Walter B. Sturek

Exterior Ballistics Laboratory

RDT&E Project No. 1T061102A33D

ABERDEEN PROVING GROUND, MARYLAND

BALLISTIC RESEARCH LABORATORIES

REPORT NO. 1649

WBSturek/lca
Aberdeen Proving Ground, Md.
May 1973

BOUNDARY LAYER STUDIES ON A SPINNING CONE

ABSTRACT

An experimental investigation of the effects of spin induced distortion of the boundary layer on a spinning 10° half angle cone at Mach 2, 3 and 4 is reported. The profile of the location of boundary layer transition has been determined completely about the surface of the cone model from spark shadowgraphs. These spark shadowgraphs were taken with the model mounted on an offset strut which was rolled incrementally in azimuth to reveal the entire surface of the model. The profile of the boundary layer thickness at the base of the cone has also been determined from the spark shadowgraphs. Strain gage balance measurements of Magnus and normal force were made for three significantly different boundary layer configurations and confirm the extreme sensitivity of Magnus to boundary layer configuration.

TABLE OF CONTENTS

LIST OF ILLUSTRATIONS

LIST OF SYMBOLS

C_{M_N}	$\frac{M_N}{qSD\ell}$
C_{M_Y}	$\frac{M_Y}{qSD\ell}$
C_N	normal force coefficient, F_N/qS
C_Y	Magnus (side) force coefficient, F_Y/qS
D	diameter of base of cone, 7.779 cm
F_N	normal force
F_Y	side force
ℓ	model length, 22.047 cm
M	Mach number
M_N	pitching moment, referenced to base of cone
M_Y	yawing moment, referenced to base of cone
P	spin rate, radians per second
q	dynamic pressure, $\rho V^2/2$
Re_ℓ	Reynolds number, $\rho V\ell/\mu$
S	reference area, base of cone, $\pi D^2/4$
V	free stream velocity
α	angle of attack
δ	boundary layer thickness
δ^*	boundary layer displacement thickness
ϵ	standard error of estimate
μ	viscosity
ρ	density

LIST OF SYMBOLS (Continued)

ϕ azimuthal angle, see Figure 2

ω spin rate, RPM

I. INTRODUCTION

The Magnus force is a side force which occurs on a spinning projectile in flight at angle of attack. Figure 1 illustrates the orientation and sign convention of the normal and side forces on a projectile. This side force and its associated moment are usually small; however, the effect of the Magnus force is an important consideration since it acts to undamp the projectile throughout the flight.

Insufficient experimental data are available to provide proper understanding of the parameters governing the Magnus force. Since the Magnus force is usually small compared to the normal force and the model must be spun to high rotational speeds, obtaining measurements of the Magnus force is a difficult task.

Theoretical analyses of the flow over a spinning body at angle of attack are not sufficiently general in application to be useful in the design of artillery projectiles and missiles. The theoretical solutions available are perturbation analyses and, as such, are valid only for small angle of attack and small spin rate. These analyses include two flow cases: (1) the incompressible flow over a spinning cylinder[1,2,3]* oriented longitudinally with the flow; and (2) supersonic flow over a spinning cone[4]. These analyses model the Magnus force as being caused by spin induced distortion of the boundary layer. The Magnus force calculated according to this model is very small. Jacobson[3] suggests that a more critical case would be where transition of the boundary layer from laminar to turbulent occurs on the body. In this case, spin induced distortion would affect the location of boundary layer transition as well as the development of the boundary layer. This would presumably result in a much larger force.

The objectives of the experimental effort reported here are to: (1) obtain data which will be of value in guiding the development of a useful theoretical treatment of the flow over a spinning body of revolution, and (2) verify the significance of the boundary layer configuration--laminar, transitional, turbulent--on the resulting Magnus force. A cone model was chosen for this experiment since its shape offers convenient simplification in the equations of motion, and also because accurate solutions of the inviscid supersonic flow over a cone are available[6].

II. THE EXPERIMENT

A. Flow Visualization

Normally, the flow along a model mounted in a wind tunnel is visible at only two locations on the model surface--the top and the

* *References are listed on page 17.*

bottom. Using an offset strut and rolling the model incrementally about the axis of the strut enables the entire surface of the model to be viewed. This technique has been applied to obtain spark shadowgraphs of the flow about the entire circumference of a 10° half angle cone model with a 7.779 cm diameter base for the following test conditions: $M = 2$, $\alpha = 2°$ and $4°$; and $M = 3$, $\alpha = 2°$; at spin rates from 0 to 30,000 RPM.

Shadowgraphs were taken at 15° increments in azimuth. Pictures were obtained as the model spun down from a high spin rate. In addition, some data were obtained while the model was held at a constant spin rate. The data obtained at a constant spin rate were more consistent than that obtained while the model was coasting down in spin rate. Figure 2 shows the coordinate system and sign convention used. An example of the shadowgraphs obtained is shown in Figure 3. In this case the wind-side boundary layer is completely laminar, and transition to turbulence on the lee-side takes place 35% of the distance from the tip of the cone to the base.

B. Force Measurements

Measurements of Magnus and normal force have been obtained using the strain gage balance technique. Data have been obtained for tunnel operating conditions duplicating that for the spark shadowgraphs and, in addition, at lower values of tunnel total pressure to yield significantly different boundary layer configurations on the model. The measurements were made while holding the model at a fixed angle of attack. The model was spun up to 35,000 RPM, and data were recorded on magnetic tape at one second intervals as the model coasted down to zero spin. The recorded data were reduced directly from the magnetic tape using a Magnus data reduction program on the BRL digital computer.

An example showing the scatter experienced in the individual data points is given in Figure 4. The data shown are corrected to zero at zero spin. The standard error of estimate (the root-mean-square of the deviations of the data about a straight line fitted to the data) is indicated for each set of data by epsilon (ε). The uncertainty in the determination of C_Y is estimated to vary from $\pm$ 0.0002 for $C_Y > 0.002$ to $\pm$ 0.00005 for $C_Y < 0.002$.

C. Test Facility

The test facility used for these tests is Supersonic Wind Tunnel No. 1 of the Ballistic Research Laboratories. This facility is a continuous flow, symmetric, flexible nozzle wind tunnel with a test section size of 38 x 33 cm. The tunnel total temperature was nominally 308 K and the tunnel total pressure was varied from .6 atm. to 4.6 atm.

III. RESULTS AND DISCUSSION

A. Boundary Layer Transition

The location of boundary layer transition completely about the circumference of the cone model was determined from the spark shadowgraphs. The position of transition was identified as the first indication of a change in the appearance of the laminar boundary layer. This criteria was used because it was easier to identify in the shadowgraphs than, say, the location of the boundary layer becoming fully turbulent. No attempt has been made to relate the location of boundary layer transition determined as indicated above with that determined by other instrumentation.

An example of the transition data is shown in Figure 5 in the form of pictures of two cone models which have been painted to reveal the regions of laminar and turbulent boundary layer--white represents laminar and black represents turbulent. These data are for $M = 2$ and $\alpha = 4°$. The region of laminar boundary layer is seen to be distorted in the direction of model rotation by spin. The transition data are shown plotted in Figures 6, 7 and 8 such that the distance from the center of the circle to the location of transition represents the distance from the tip of the cone along a ray of the cone to the position of boundary layer transition. The trends indicated are: (1) transition is delayed when the spin velocity is in the same direction as the cross-flow velocity; and (2) transition occurs sooner when the spin velocity opposes the cross-flow velocity. It is interesting to note that the data for $M = 3$ indicate an enlarged region of laminar boundary layer compared to that for $M = 2$; however, the trend of the data with spin is identical.

B. Boundary Layer Thickness

In addition to the location of boundary layer transition, measurements of the apparent boundary layer thickness at the base of the cone were made from the spark shadowgraphs. These data are shown in Figures 9. For zero spin, the profile is symmetric. As spin is increased, the profile of the thickness of the boundary layer becomes increasingly asymmetric. Another trend indicated is that the thickness of the boundary layer at the base becomes more uniform about the circumference as the spin rate is increased.

C. Wall Pressure Distribution

An estimate has been made of the change in pressure distribution about the cone model caused by the spin distorted boundary layer. This has been accomplished by obtaining a value of δ^*/δ from the tables in NAVORD Report 4282[5] assuming a 1/7 power law velocity profile and adiabatic wall. This ratio multiplied by the measured value of δ, the boundary layer thickness, yields a value for the displacement thickness

of the boundary layer. This value of δ^* has been added to the radius of the base of the cone and, extending a straight line to the tip of the cone, defines an effective conical body that is no longer symmetric due to the distortion of the boundary layer.

The pressure distribution as a function of effective cone angle and azimuthal position has been interpolated for in the tables published in AGARDograph 137[6]. An example of the pressure distribution obtained is shown in Figure 10. This figure shows two pressure distributions: (1) 10° cone plus boundary layer for zero spin; and (2) 10° cone plus boundary layer for a spin rate of 30,000 RPM. The pressure distribution for $\omega > 0$ is asymmetric. This is indicated by the separation of the lines at values of ϕ between 180° and 360° on the cone. The change in wall pressure indicated at $\phi = 240°$ is about 1379 dynes/cm^2. Values of Magnus and normal force coefficients have been calculated by integrating the pressure distribution about the circumference of the model. The results are discussed in the next section where the calculated value is compared to values measured using a strain gage balance.

D. Force Measurements

An example of the normal force data is shown in Figure 11. The measured values of normal force are compared to values obtained from the tables of inviscid calculations in reference 6. The agreement is excellent up to the highest value of angle of attack, 8°. This indicates the insensitivity of the normal force to boundary layer configuration.

The Magnus force measured for the case in which boundary layer transition occurred naturally about the entire surface of the model is shown in Figure 12. The data shown are curve fits of the individual data points and are corrected to zero at zero spin rate. The Magnus force is seen to be extremely small for this boundary layer configuration; and, comparing the value for $\alpha = 4°$ at the highest spin rate with the normal force for $\alpha = 4°$, it is seen that the Magnus force is approximately 2% of the normal force.

Also shown in Figure 12 are values of Magnus force coefficient calculated from the pressure distribution as discussed earlier. The calculated Magnus coefficients exhibit poor agreement with the measured values. Also, the trends indicated by the measured values in angle of attack and spin rate are not indicated by the calculated values. This is probably due to the crudeness of the calculation; however, it could also indicate that mechanisms in addition to the distortion of the boundary layer play a significant role in causing the side force. Additional mechanisms include asymmetry in the pressure distribution through the boundary layer and asymmetry in the wall shear stress.

Data are compared in Figure 13 for different boundary layer configurations. The solid line represents data obtained at a low value of tunnel total pressure for which the boundary layer remained laminar

on the wind-side while transition to turbulence occurred near the tip of the cone for the lee-side. This resulted in a large difference in thickness of the boundary layer at the base of the cone from the wind to the lee-side (lee: $\delta \approx .025$-cm; wind: $\delta \approx .002$-cm). The broken line represents data obtained for tunnel conditions that resulted in transition to turbulence occurring completely about the model surface before reaching the base. It is seen that the configuration with the greatest difference in boundary layer thickness from the wind to the lee-side results in the largest Magnus force. For the configurations shown, the Magnus force is changed by a factor of eight by a change in Reynolds number of only a factor of three.

In Figure 14, a comparison similar to that in Figure 13 is made. The comparison in Figure 14 is between a boundary layer tripped to turbulent by a sand strip placed one-inch from the tip of the cone and a boundary layer which remained laminar on the wind-side. The sand strip was one-quarter-inch wide and consisted of #80 sand grit. Again, the boundary layer configuration resulting in the greatest difference in boundary layer thickness from the wind to the lee-side results in the largest Magnus force. A complete tabulation of the strain gage balance data is given in Table 1. In comparing the measured Magnus force coefficients obtained in this experiment to those published in reference 7, no agreement either in trend or magnitude is noted for the data at $M = 2$, $Re_{\ell} \approx 2 \times 10^6$. However, the data from reference 7 is in reasonable agreement with the data of this experiment for $M = 3$, $Re_{\ell} \approx 2 \times 10^6$. Close agreement for Magnus force between experiments conducted at different test facilities, especially at tunnel operating conditions which yield laminar or transitional boundary layer configurations, should not be expected due to the extreme sensitivity of the Magnus force to boundary layer configuration.

IV. CONCLUSIONS

The following conclusions have been reached upon examination of the experimental data.

(1) The distortion of spin on the location of boundary layer transition reveals the trends that transition is delayed where the cross-flow velocity adds to the spin velocity and occurs earlier where the cross-flow velocity opposes the spin velocity.

(2) Spin induced distortion of the boundary layer results in asymmetry in the profile of the boundary layer thickness.

(3) The Magnus force is caused, at least in part, by spin induced distortion of the boundary layer.

(4) The Magnus force is extremely sensitive to boundary layer configuration. The Magnus force is greatest for the boundary layer configuration that has the greatest difference in thickness of the boundary layer from the wind to the lee-side.

This experiment has been conducted with the intent of providing experimental data which would be of value in guiding the development of a useful theoretical analysis. The data indicate trend and magnitude of effects that a generally applicable analysis must be capable of predicting. Much additional data are needed. Detailed surveys of boundary layer characteristics on a spinning body of revolution are of particular interest.

REFERENCES

1. J. C. Martin, "On Magnus Effects Caused by Boundary Layer Displacement Thickness on Bodies of Revolution at Small Angles of Attack," BRL Report 870 (Revised), U.S. Army Ballistic Research Laboratories, Aberdeen Proving Ground, Maryland, June 1955. AD 72055.

2. H. R. Kelly and G. R. Thacker, "The Effect of High Spin on the Magnus Force on a Cylinder at Small Angles of Attack," NAVORD Report 5036, U.S. Naval Ordnance Test Station, China Lake, California, February 1956.

3. Ira D. Jacobson, "Influence of Boundary Layer Transition on the Magnus Effect on a Spinning Body of Revolution," PhD Dissertation, University of Virginia, June 1970.

4. R. Sedney, "Laminar Boundary Layer on a Spinning Cone at Small Angles of Attack in a Supersonic Flow," *Journal of the Aeronautical Sciences*, Vol. 24, No. 6, June 1957, pp. 430-436.

5. Jerome Persh and Roland Lee, "Tabulation of Compressible Turbulent Boundary Layer Parameters," NAVORD Report 4282, U.S. Naval Ordnance Laboratory, White Oak, Maryland, May 1956.

6. D. J. Jones, "Tables of Inviscid Supersonic Flow About Circular Cones at Incidence, $\gamma = 1.4$," AGARDograph 137, November 1969.

7. W. H. Curry, J. F. Reed and W. C. Ragsdale, "Magnus Data on the Standard 10° Cone Calibration Model," SC-DC 71 3821, Sandia Laboratories, Albuquerque, New Mexico, March 1971.

Table 1. Strain-Gage Balance Tabulated Data

M	P_o cm Hg	T_o °K	α	C_Y (1) B	C_Y (1) C	C_{M_Y} (1) D	C_{M_Y} (1) E	Boundary Layer (2-5) Wind	Boundary Layer (2-5) Lee	$Re_\ell \times 10^{-6}$
2	170	308.0	2.01	-.000132		.000462		See Figures 6A - 6D		5.91
2	175	307.6	4.06	-.001190		-.000519		See Figures 7A - 7D		6.10
2	175	307.6	6.11	-.002214		-.001490		(70)	(22)	6.10
2	175	307.6	8.14	-.00330		-.002367		(73)	(22)	6.10
2	170	307.7	- 2.05	.000423		-.000273		See Figures 6A - 6D		5.92
2	175	307.6	- 4.09	.001465		.000852		See Figures 7A - 7D		6.09
2	175	307.4	- 6.12	.002428		.001571		(75)	(22)	6.11
2	50	305.4	1.99	-.006095		.002326		L	L	1.76
2	50	305.4	4.03	-.01436	.01314	.01404	-.02545	L	(27)	1.76
2	50	305.4	6.03	-.01552	.01169	.002299	-.001026	L	(22)	1.76
2	50	305.3	- 2.02	.007888		-.001285		L	L	1.76
2	50	305.3	- 4.04	.01719	-.01704	-.01028	.02069	L	(43)	1.76
2	175	311.3	2.03	-.000889		.000055		TR (33)	TR (22)	5.99
2	175	312.8	4.07	-.00201		-.001157		TR (41)	TR (16)	5.93
2	175	311.9	- 2.03	.001055		-.000086		TR (22)	TR (22)	5.95
2	175	311.3	- 4.06	.002174		.000893		TR (39)	TR (18)	5.96
3	230	308.1	2.01	-.001955		-.000566		See Figures 8A - 8D		4.80
3	250	307.8	4.05	-.001279		-.000451		(97)	(18)	5.22
3	250	307.8	6.09	-.003169	.004279	-.001915	.001089	(99)	(18)	5.20
3	250	308.5	8.11	-.002869	.001599	-.001307	-.002932	L	(18)	5.19
3	250	309.1	10.13	-.005017	.005988	-.003675	.002035	L	(18)	5.18
3	230	307.7	- 2.03	.001825		.000649		See Figures 8A - 8D		4.81
3	250	308.8	- 4.05	.001581		.000711		(96)	(22)	5.18
3	90	304.8	2.01	-.003805		.001915		L	(66)	1.93
3	90	304.7	4.03	-.005343		.001411		L	(45)	1.94
3	90	304.8	6.05	-.006373		.000309		L	(47)	1.94
3	90	304.5	8.05	-.006749		-.000765		L	(43)	1.93
3	90	304.7	10.06	-.007616		-.001667		L	(43)	1.93
3	90	304.4	- 2.01	.004549		-.000941		L	(66)	1.93
3	90	309.6	- 4.02	.006552		-.000261		L	(45)	1.93

Table 1. Strain-Gage Balance Tabulated Data (Continued)

M	P_o cm Hg	T_o °F	α	C_Y B	C_Y C	C_{M_Y} D	C_{M_Y} E	Boundary Layer Wind	Boundary Layer Lee	$Re_\ell \times 10^{-6}$
3	250	311.2	2.00	-.000643		-.000769		TR (29)	TR (18)	5.19
3	250	311.9	4.04	-.001314		-.001290		TR (31)	TR (20)	5.14
3	250	312.0	- 2.03	.000683		-.000168		TR (27)	TR (29)	5.12
3	250	311.3	- 4.06	.001187		.000346		TR (29)	TR (24)	5.13
4	360	306.7	1.99	-.003134		-.001842		Unknown	Unknown	4.44
4	360	307.3	4.02	-.002318		-.001690		(92)	(22)	4.43
4	360	307.9	6.03	-.002144		-.001884		L	(22)	4.41

NOTES:

1. Curve fit of data is corrected to zero at zero spin. The curve fit chosen (first or second degree) was that which agreed best with the trend of the plotted data.

$$C_Y = B\,(pD/V) + C\,(pD/V)^2 \qquad C_{M_Y} = D\,(pD/V) + E\,(pD/V)^2$$

2. Boundary layer transition data was determined from spark shadowgraph for zero spin except as indicated in Figures 3A - 3L.

3. L -- indicates boundary layer remained laminar to base of cone.

4. ( ) -- transition to turbulent boundary layer occurred ( ) % of distance from the tip to the base of the cone.

5. TR ( ) -- boundary layer trip one-inch from tip of cone. Trip consisted of one-quarter-inch band of # 80 sand grit. ( ) -- indicates position on surface that the boundary layer actually became turbulent.

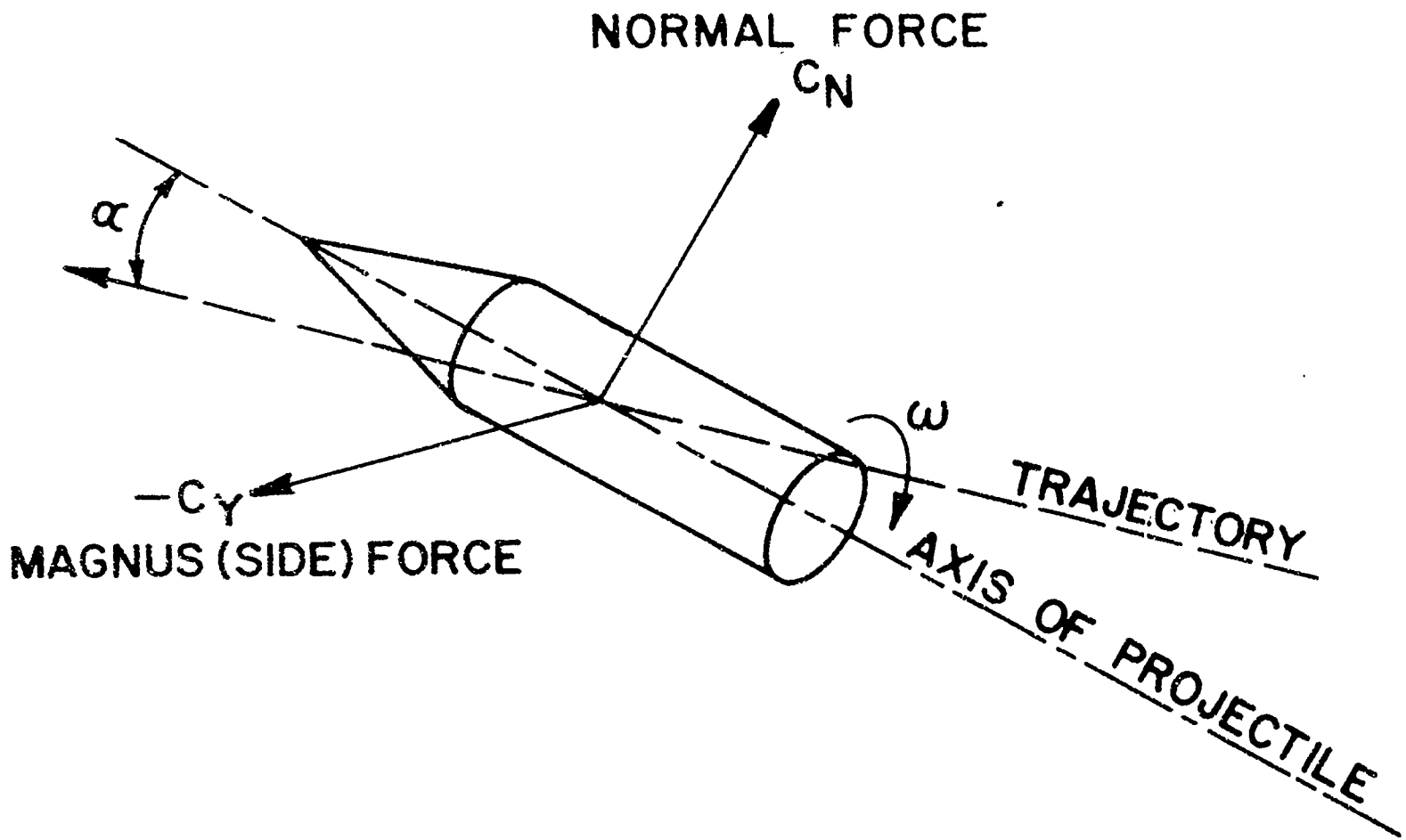

Figure 1. Magnus and Normal Forces on a Spinning Projectile

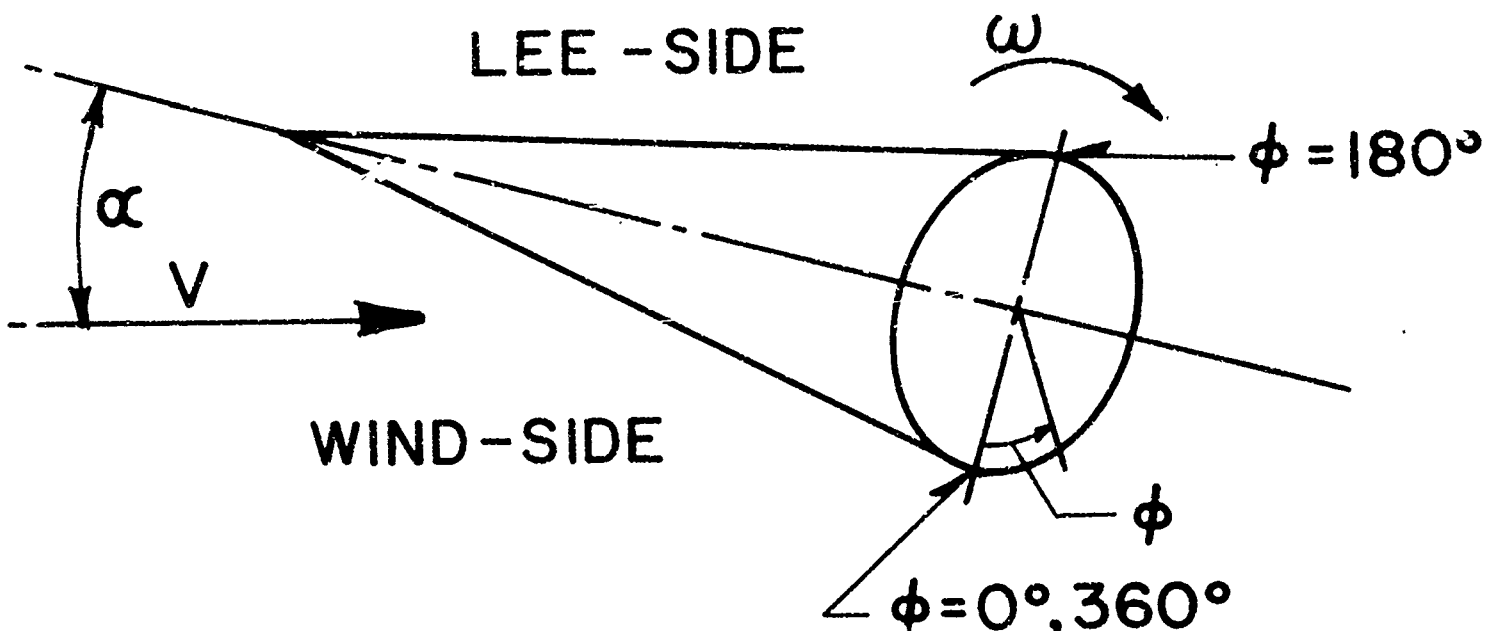

Figure 2. Coordinate System

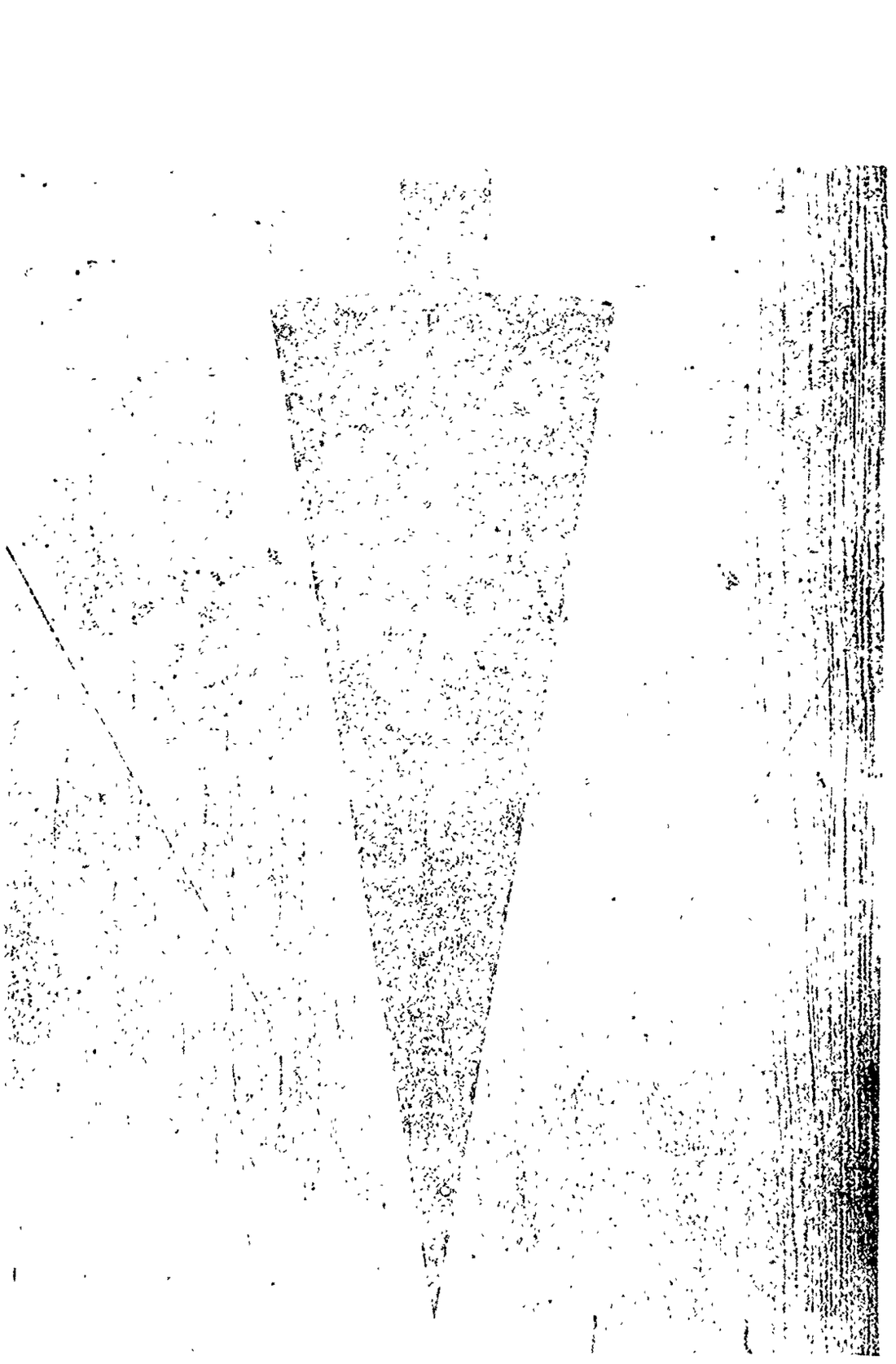

Figure 3 Shadowgraph of Flow Over the Cone Model, $\alpha = 2°$, [illegible] 10,300 PSI, $Re = 1.8 \times 10^6$

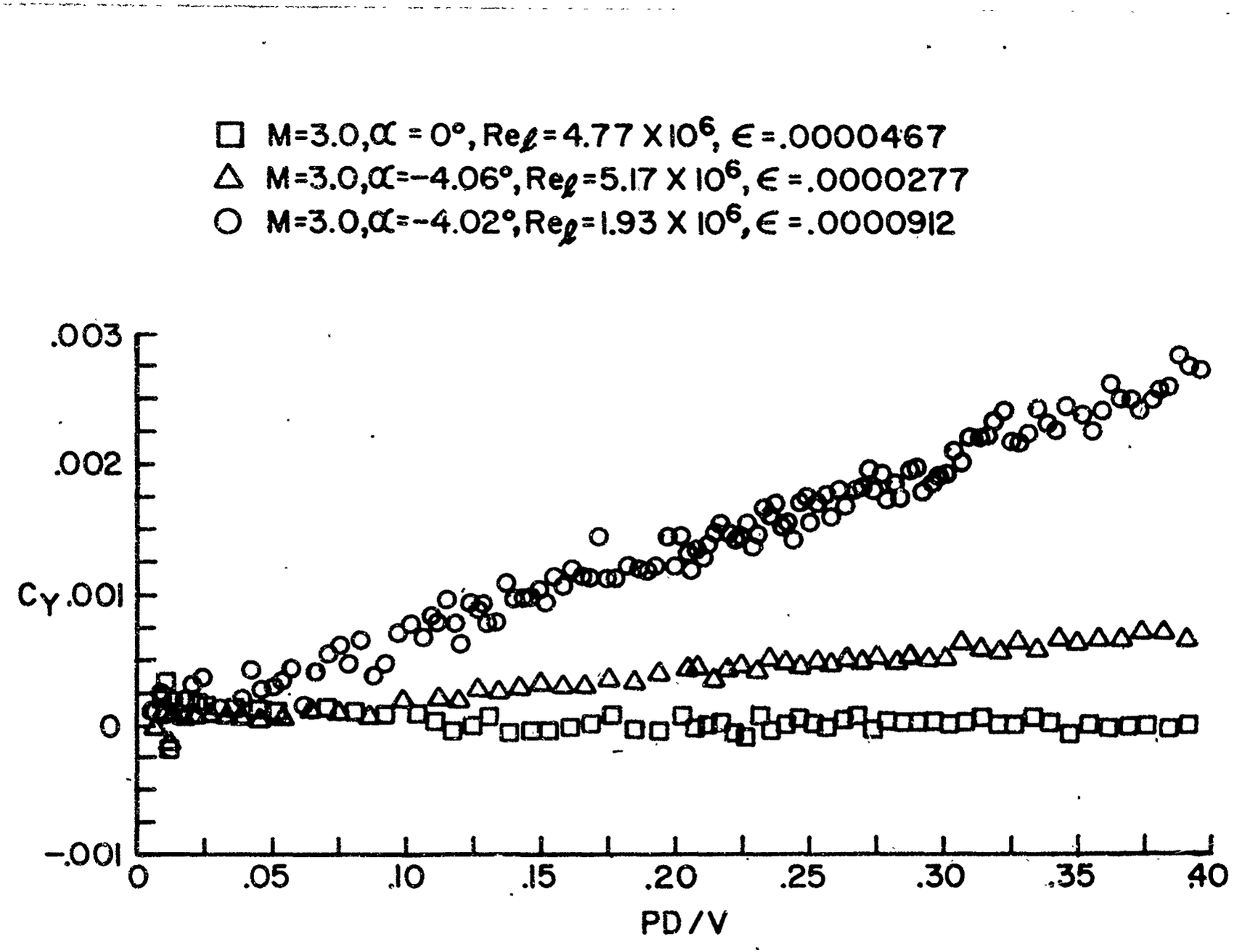

Figure 4. Magnus Coefficient Versus Spin Rate--Individual Data Points

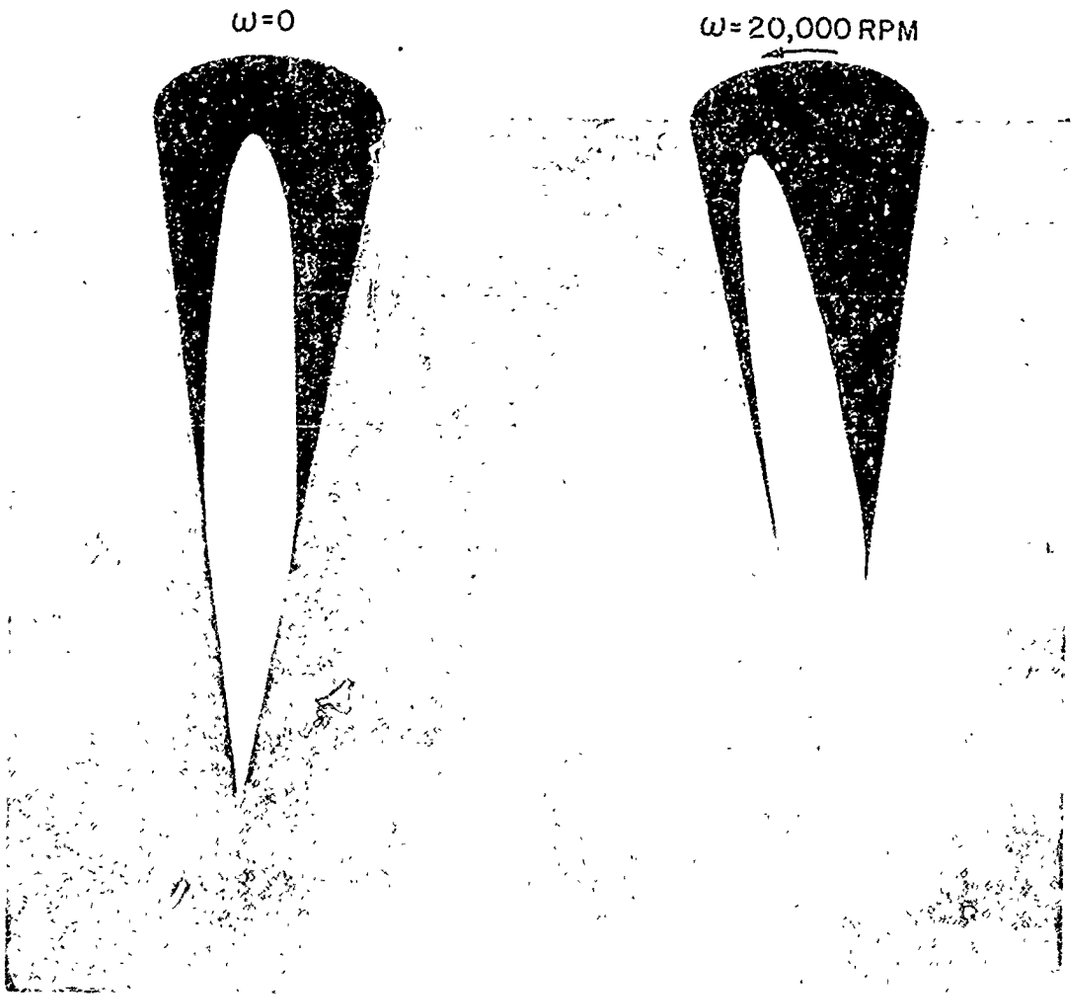

Figure 5. Cone Models Painted to Reveal Regions of Laminar (White) and Turbulent (Black) Boundary Layer, M = 2, α = 4°, $Re_{\ell} = 5.97 \times 10^6$

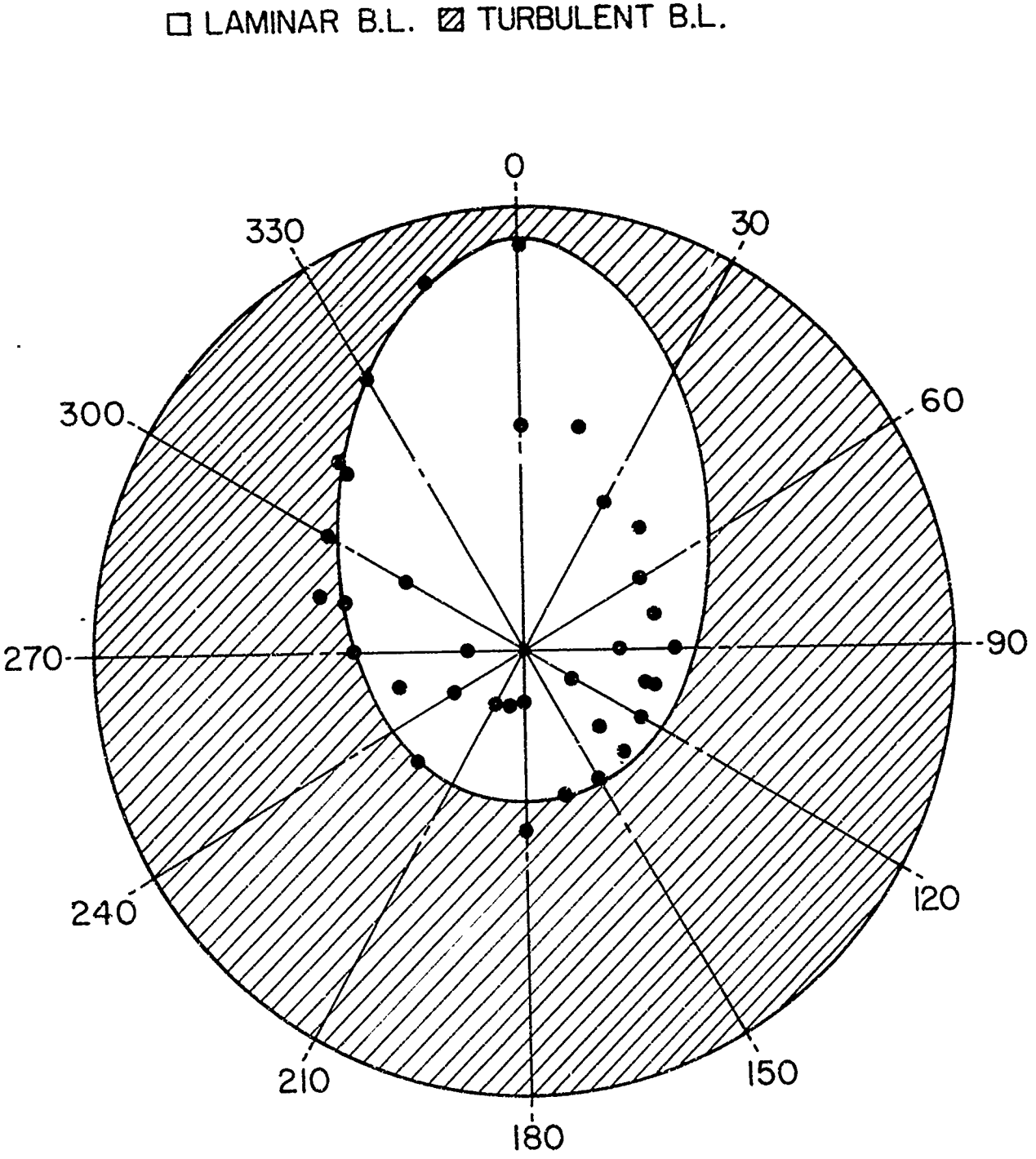

Figure 6A. Profile of Boundary Layer Transition About Circumference of 10° Cone, M = 2, α = 2°, ω = 0, $Re_{\ell} = 5.87 \times 10^6$

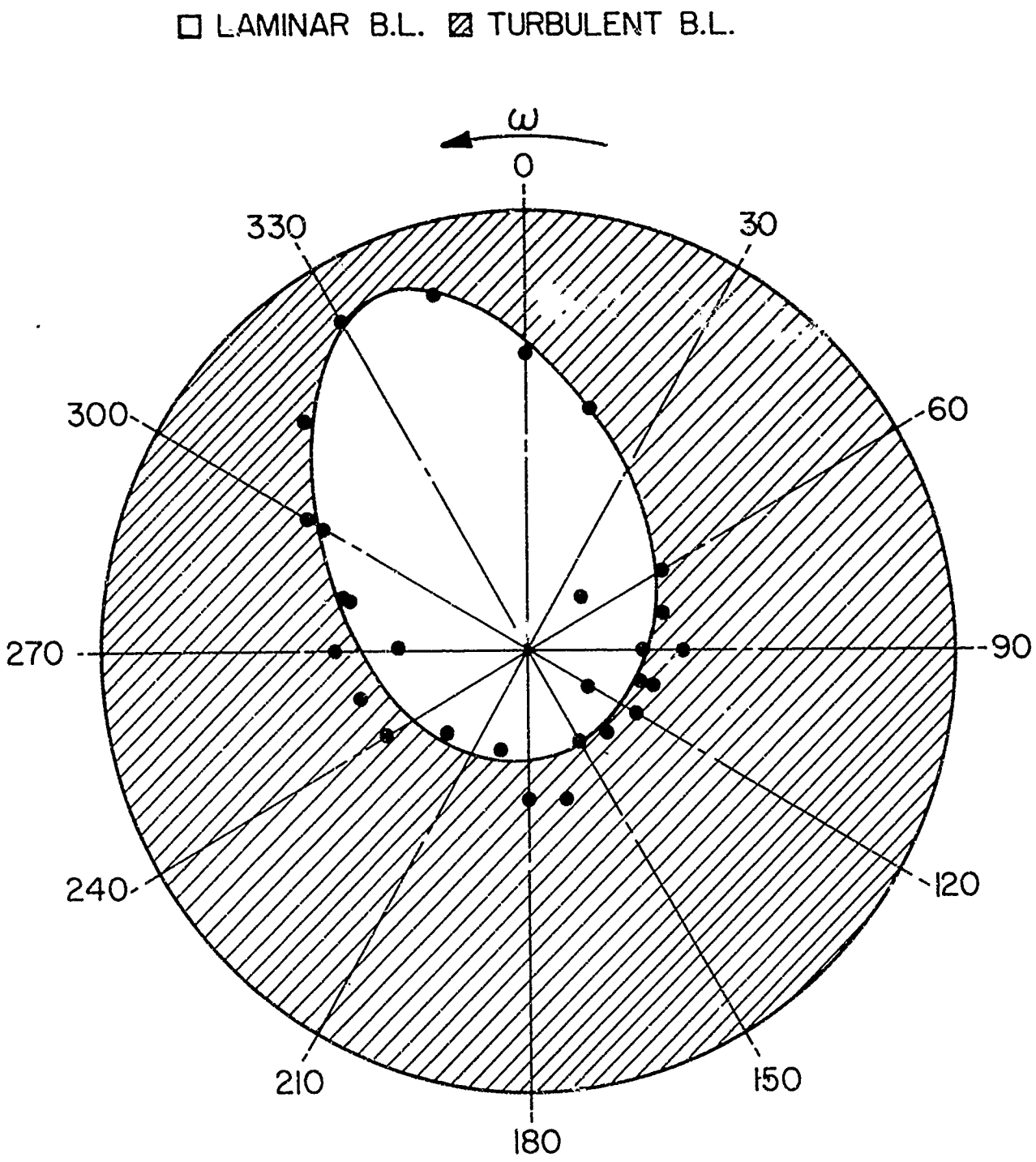

Figure 6B. Profile of Boundary Layer Transition About Circumference of 10° Cone, M = 2, α = 2°, ω = 10,000 RPM, $Re_{\ell} = 5.87 \times 10^6$

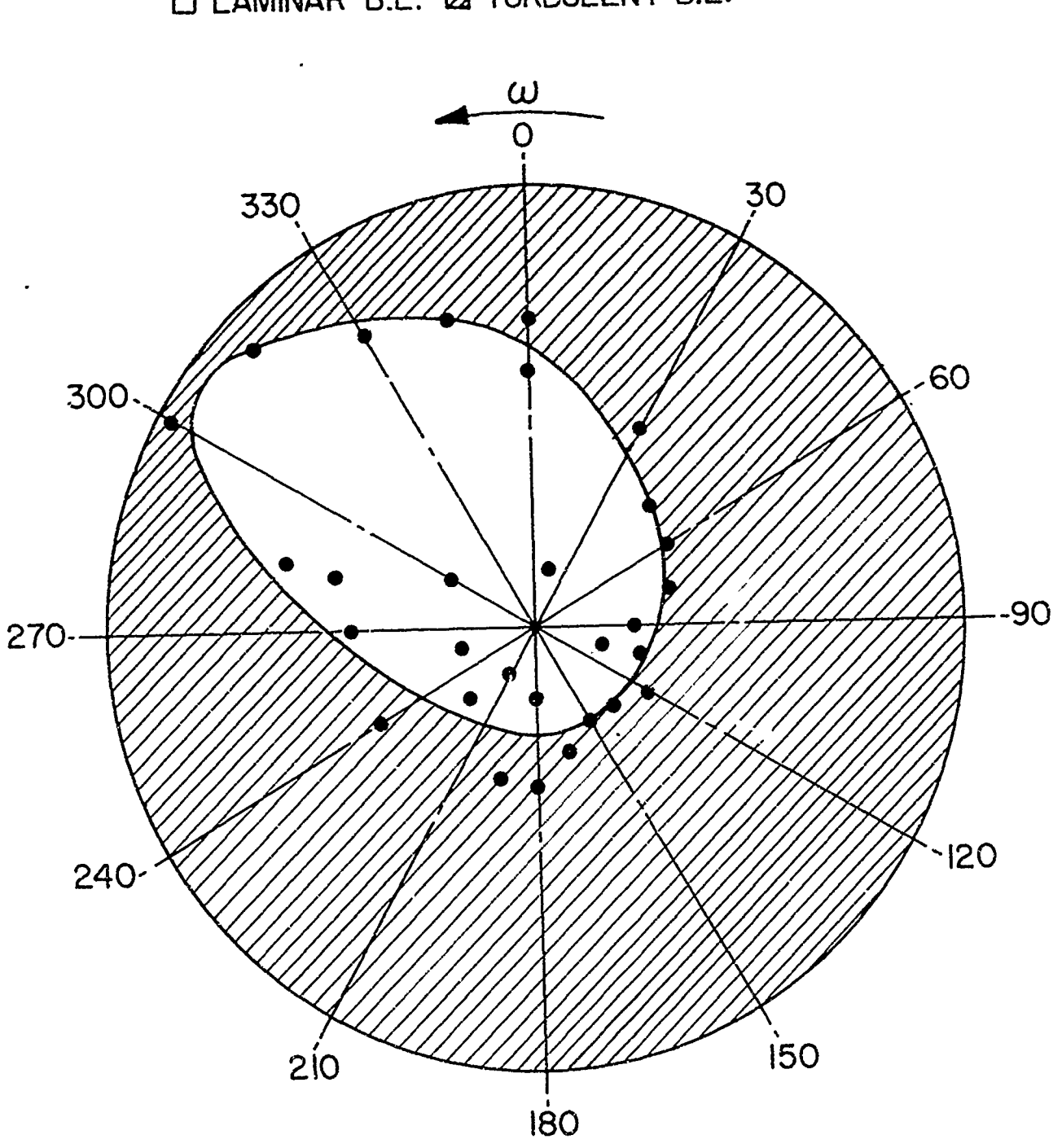

Figure 6C. Profile of Boundary Layer Transition About Circumference of 10° Cone, M = 2, α = 2°, ω = 20,000 RPM, $Re_{\ell} = 5.87 \times 10^6$

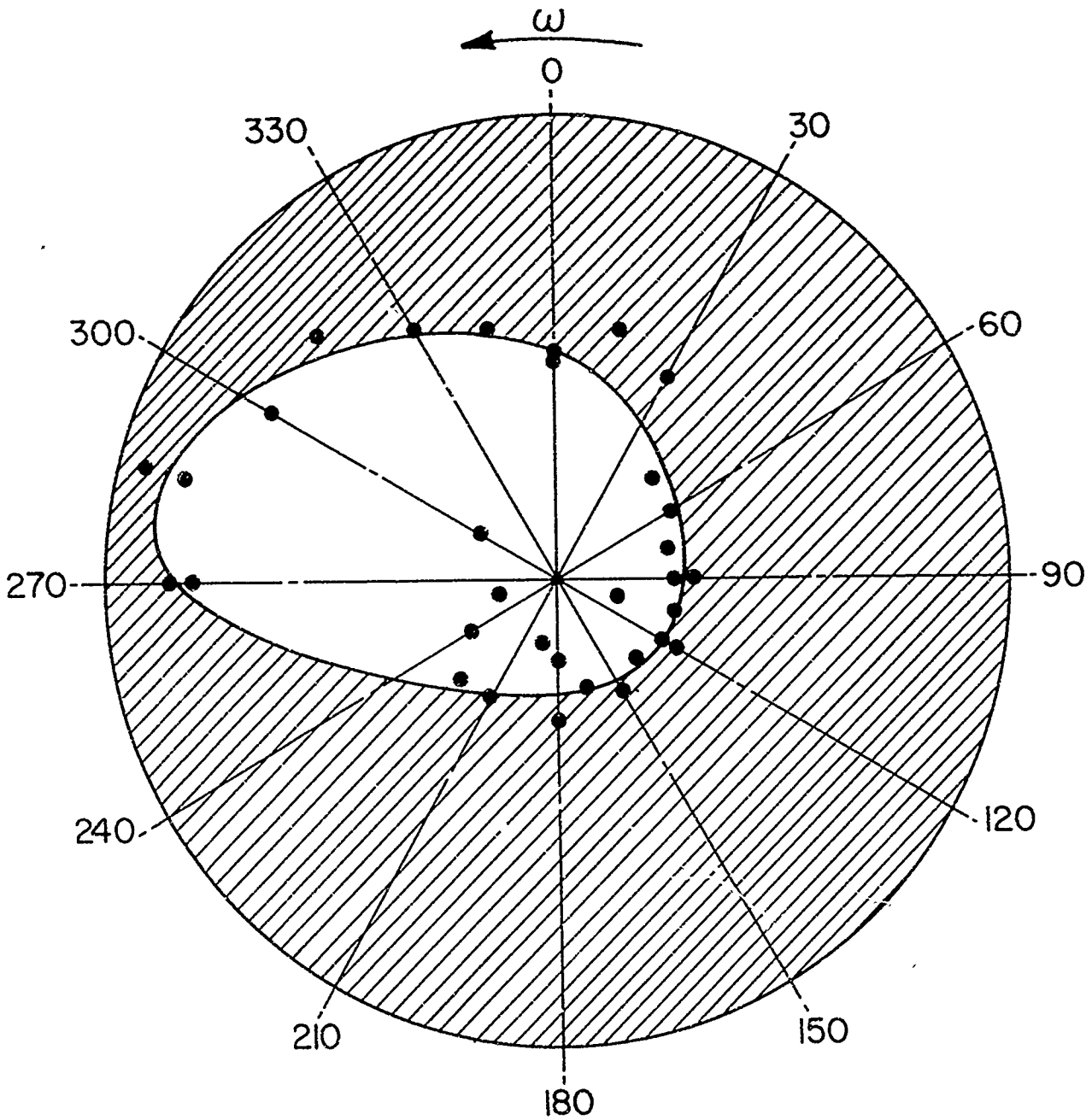

Figure 6D. Profile of Boundary Layer Transition About Circumference of 10° Cone, M = 2, α = 2°, ω = 30,000 RPM, $Re_{\ell} = 5.87 \times 10^6$

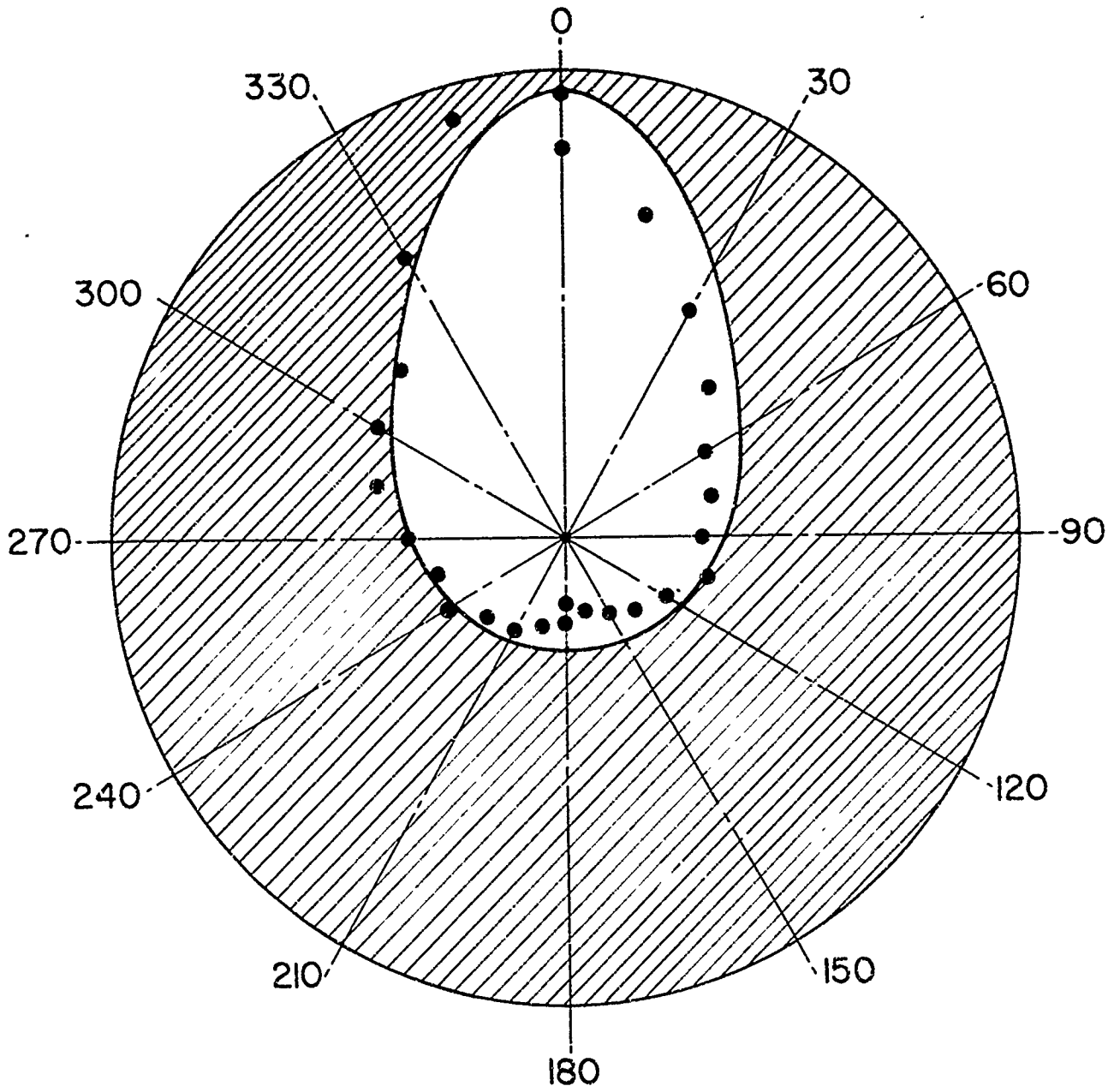

Figure 7A. Profile of Boundary Layer Transition About Circumference of 10° Cone, M = 2, α = 4°, ω = 0, Re_{ℓ} = 5.97 x 10^6

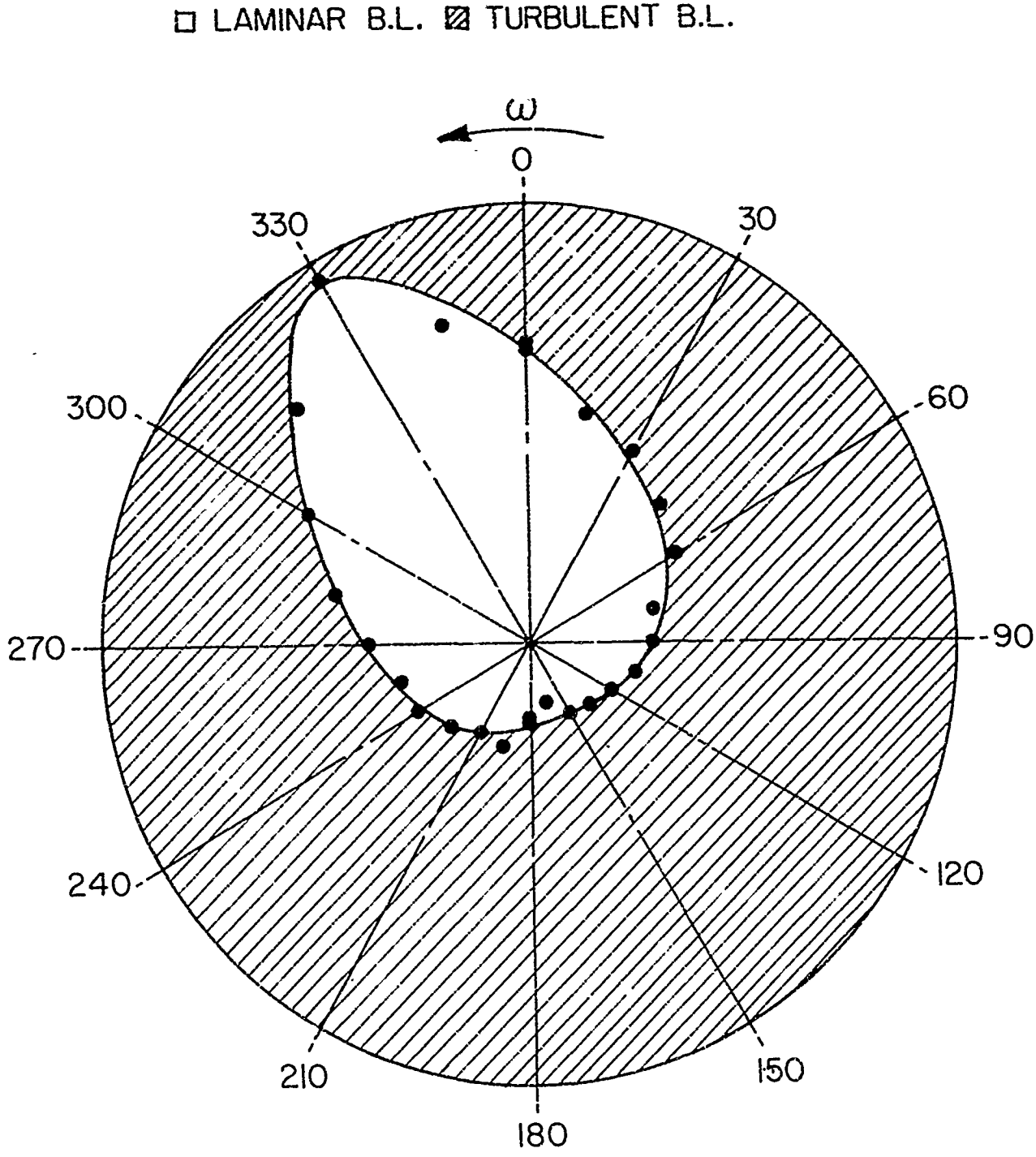

Figure 7B. Profile of Boundary Layer Transition About Circumference of 10° Cone, M = 2, α = 4°, ω = 10,000 RPM, $Re_{\ell} = 5.97 \times 10^6$

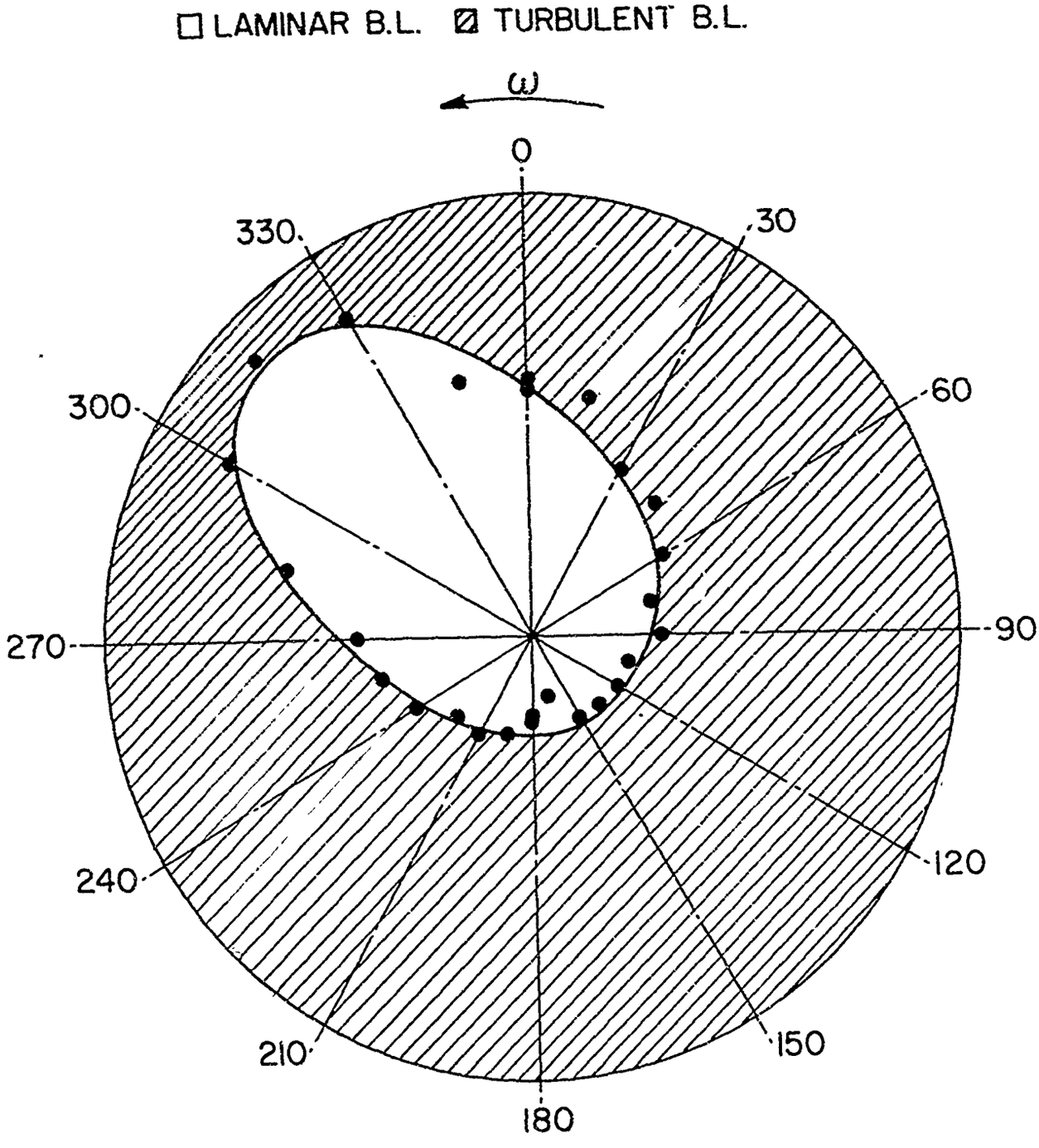

Figure 7C. Profile of Boundary Layer Transition About Circumference of 10° Cone, M = 2, α = 4°, ω = 20,000 RPM, $Re_{\ell} = 5.97 \times 10^6$

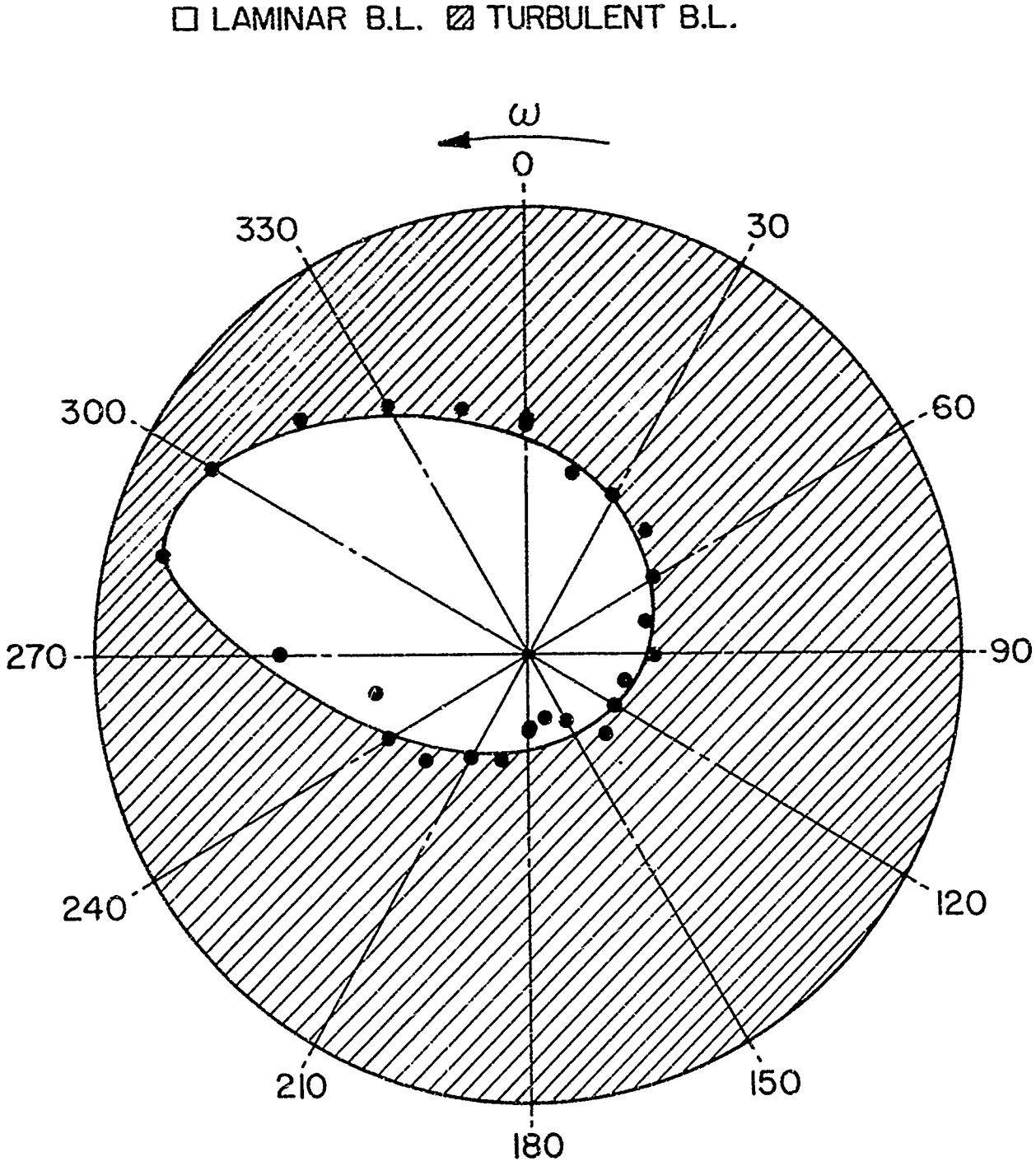

Figure 7D. Profile of Boundary Layer Transition About Circumference of 10° Cone, M = 2, α = 4°, ω = 30,000 RPM, $Re_{\ell} = 5.97 \times 10^6$

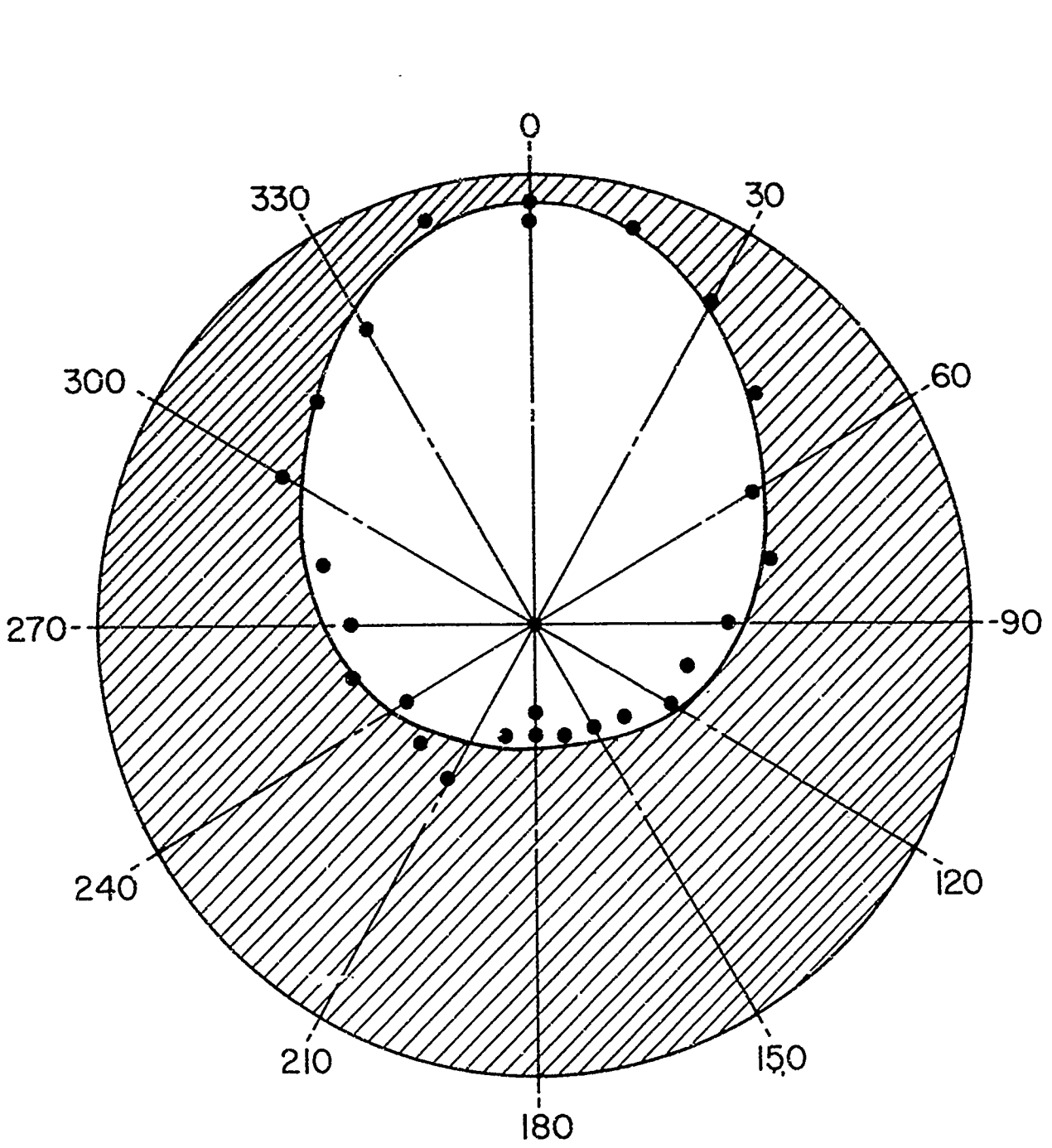

Figure 8A. Profile of Boundary Layer Transition About Circumference of 10° Cone, M = 3, α = 2°, ω = 0, Re_{ℓ} = 4.80 x 10^6

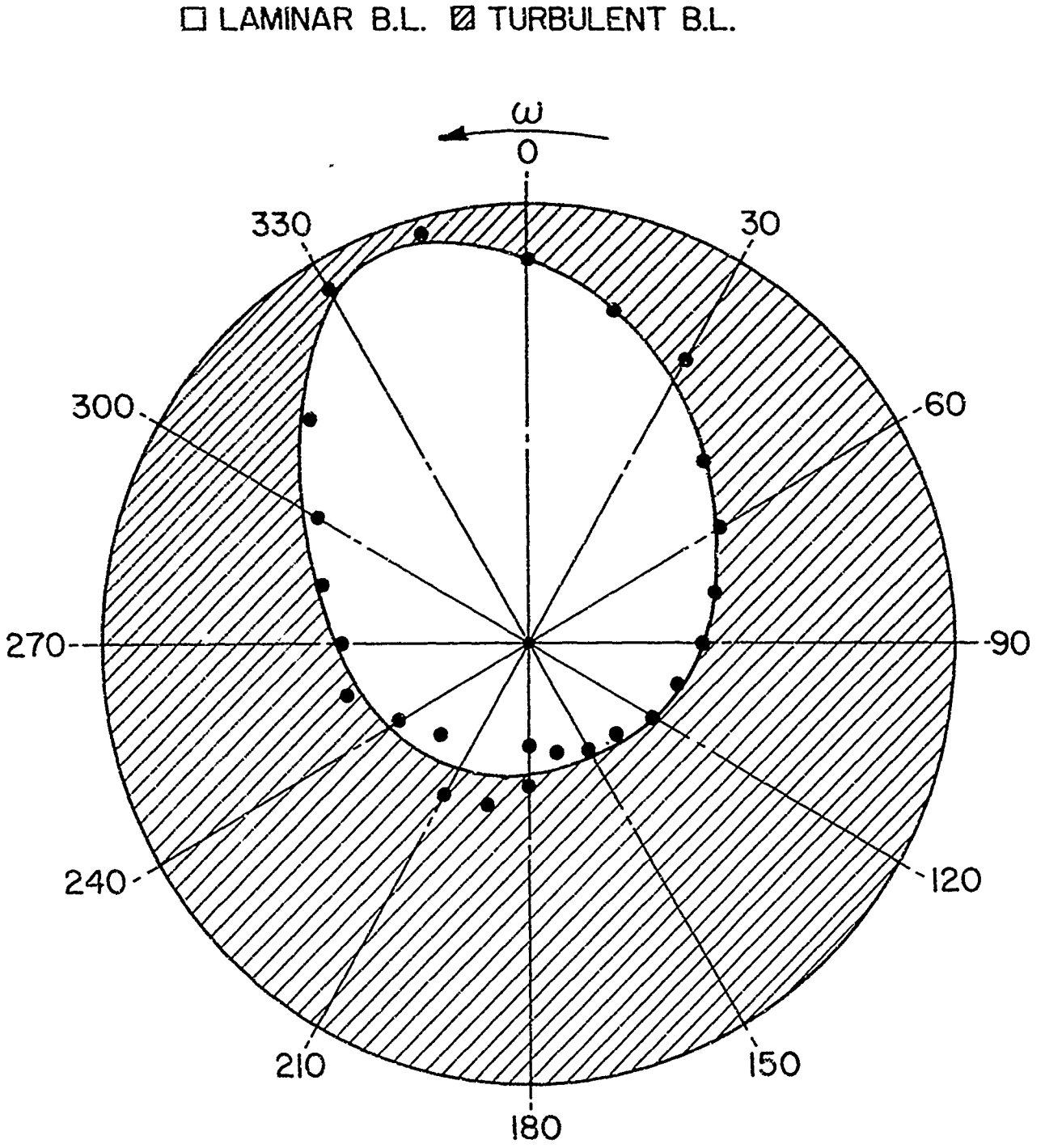

Figure 8B. Profile of Boundary Layer Transition About Circumference of 10° Cone, M = 3, α = 2°, ω = 10,000 RPM, Re_{ℓ} = 4.80 x 10^6

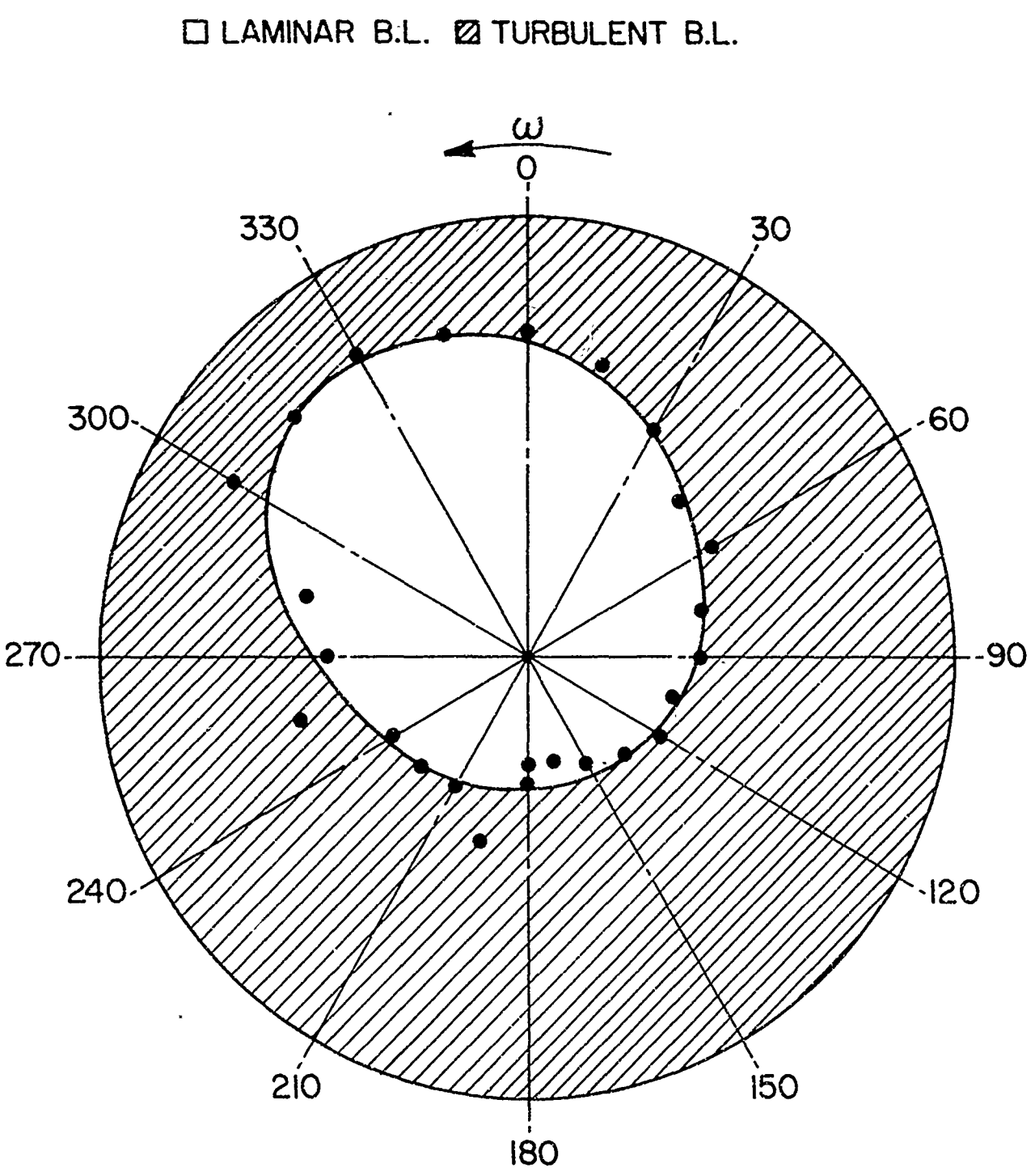

Figure 8C. Profile of Boundary Layer Transition About Circumference of 10° Cone, M = 3, α = 2°, ω = 20,000 RPM, $Re_{\ell} = 4.80 \times 10^6$

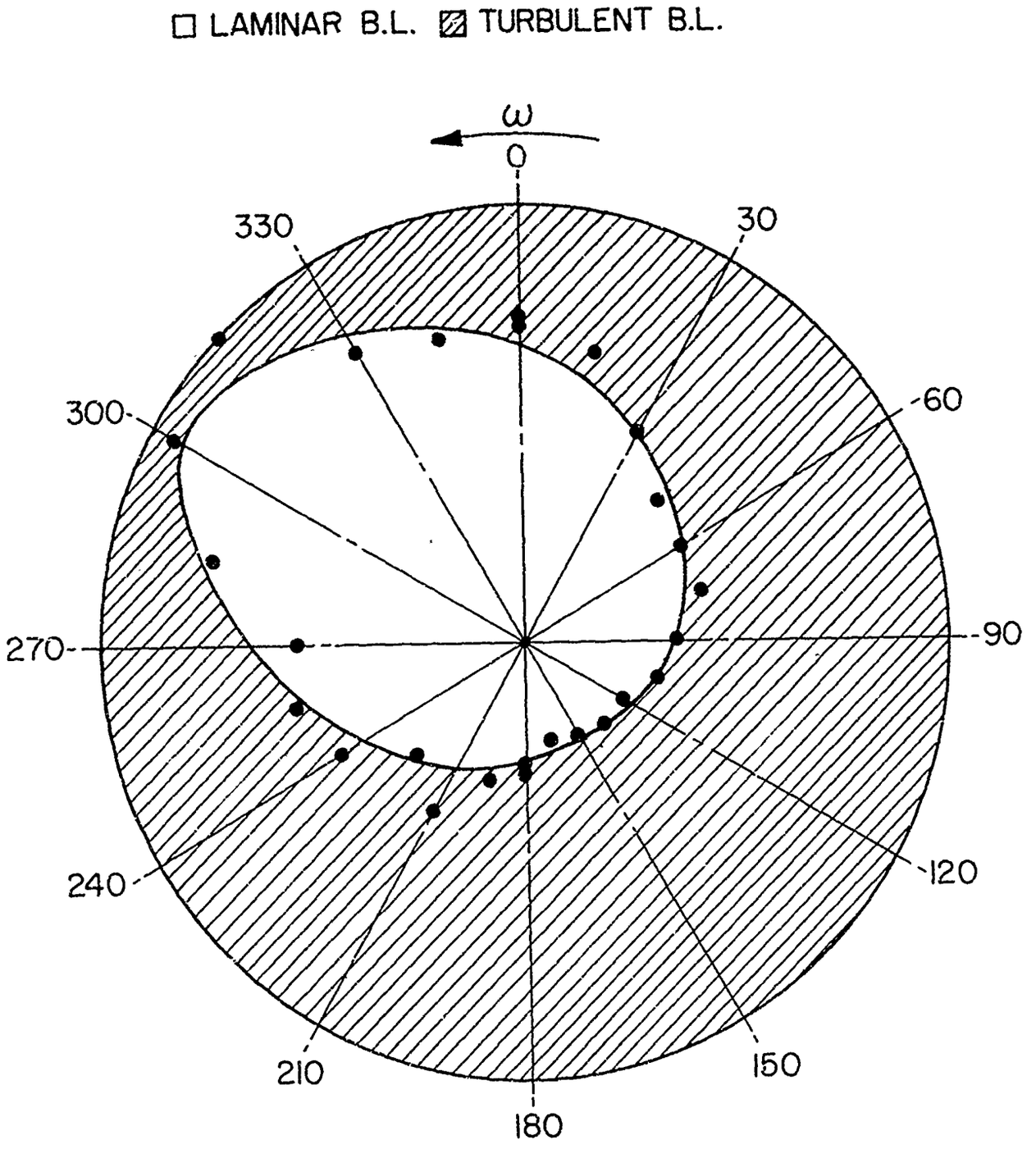

Figure 8D. Profile of Boundary Layer Transition About Circumference of 10° Cone, M = 3, α = 2°, ω = 30,000 RPM, Re_{ℓ} = 4.80 x 10^6

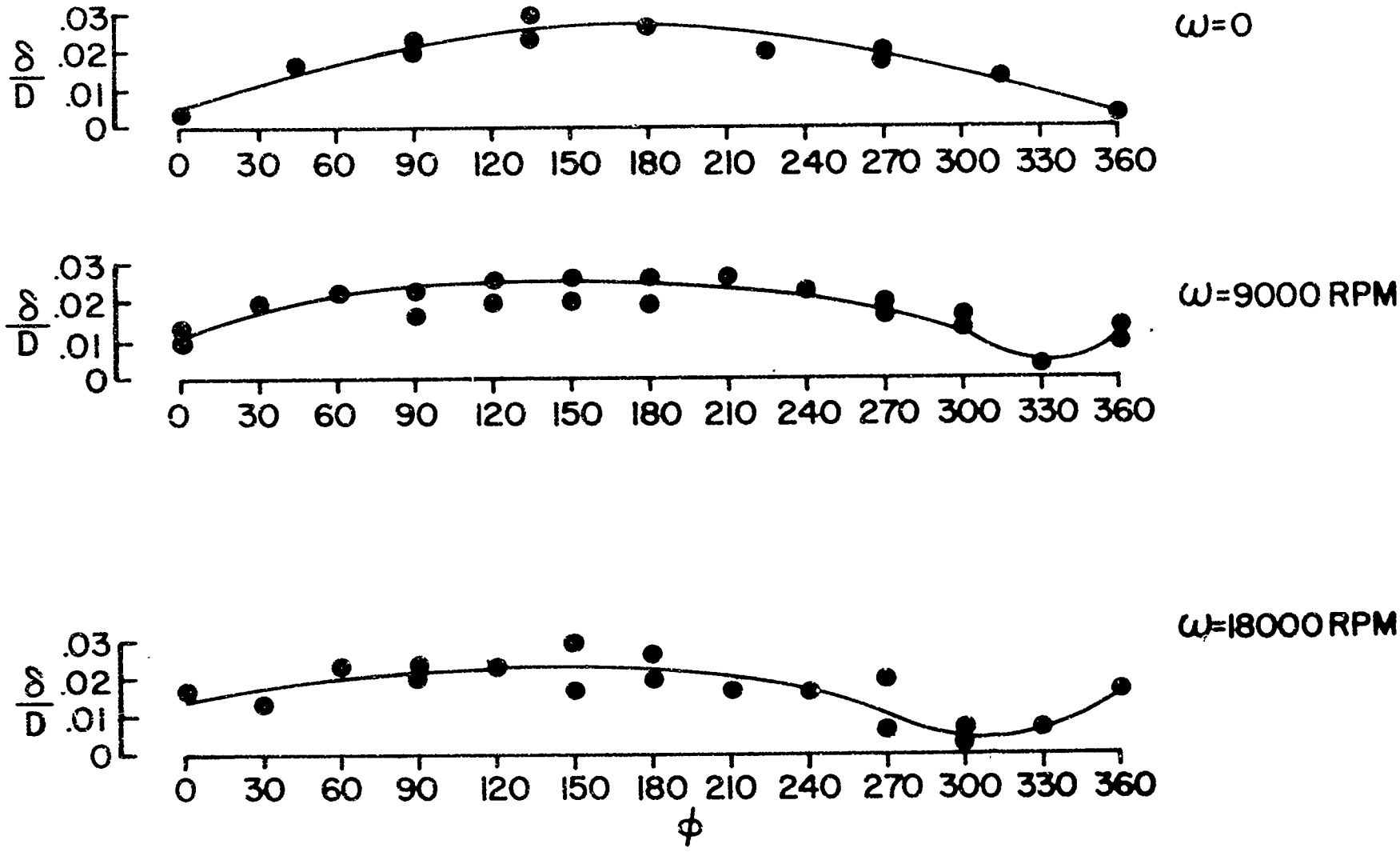

Figure 9A. Distribution of Boundary Layer Thickness About the Circumference of the Cone Model at the Base, M = 2, α = 2°, Re_{ℓ} = 4.80 x 10^6

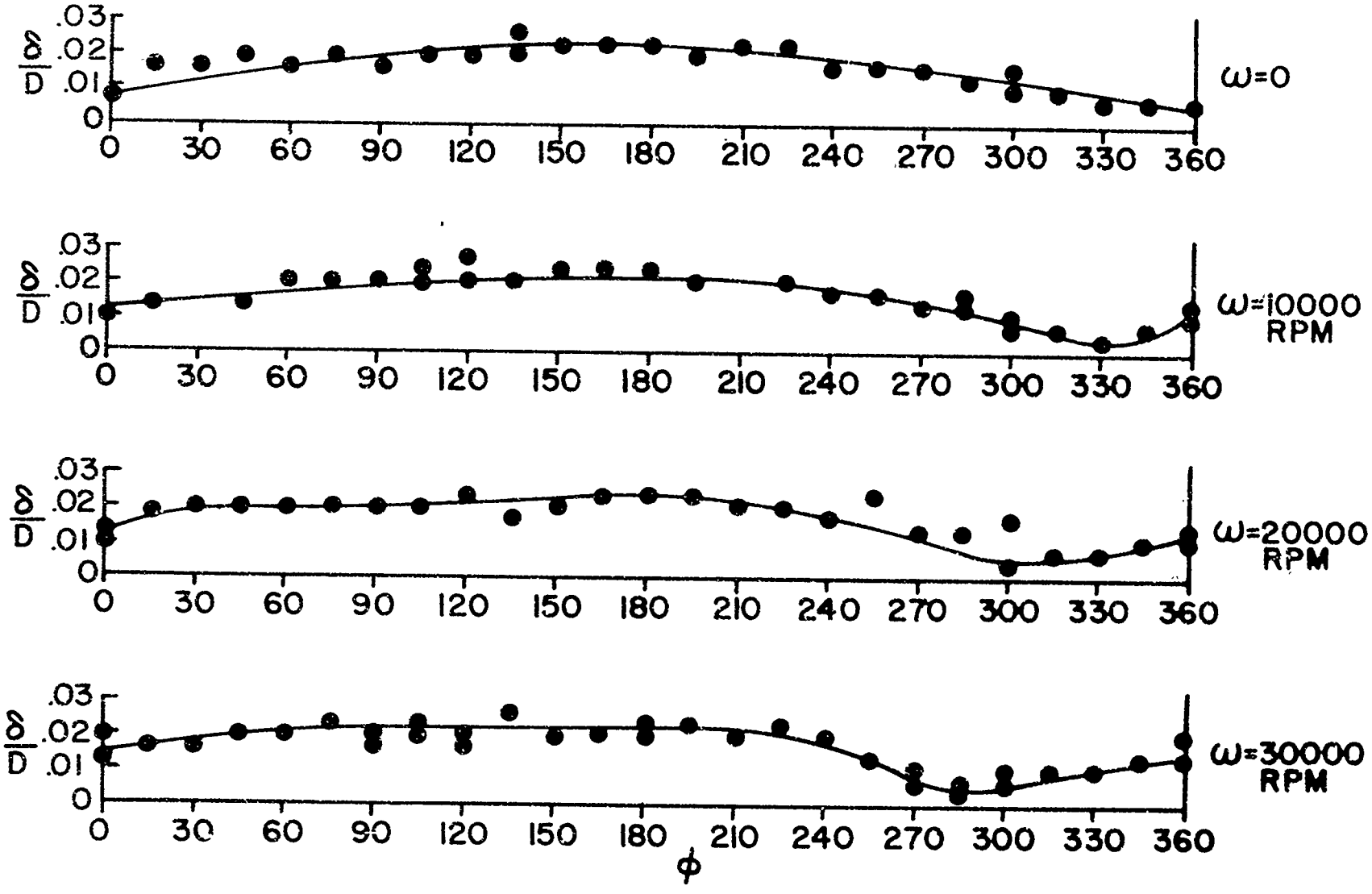

Figure 9B. Distribution of Boundary Layer Thickness About the Circumference of the Cone Model at the Base, M = 2, α = 2°, Re_{ℓ} = 5.87 x 10^6

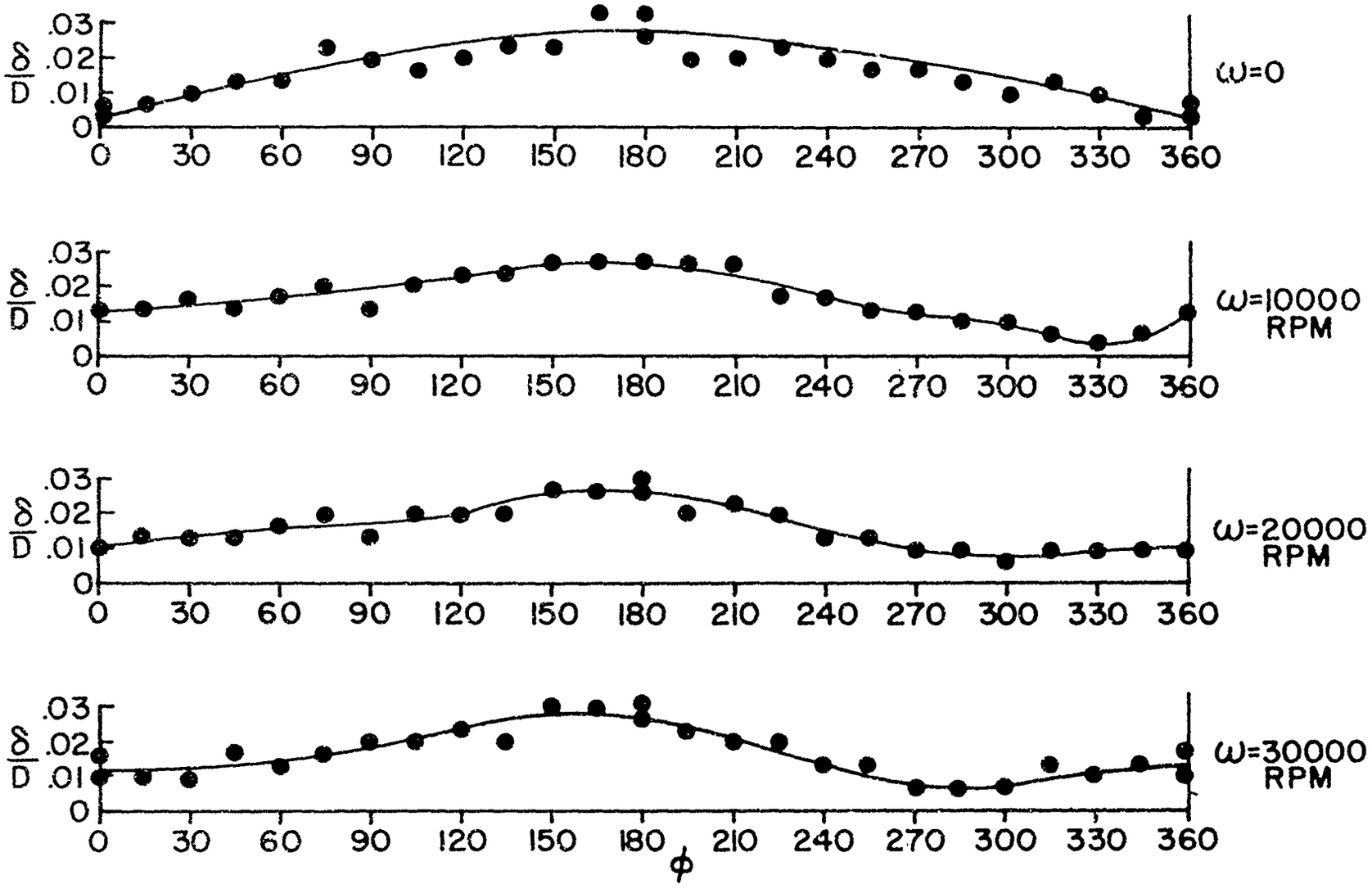

Figure 3C. Distribution of Boundary Layer Thickness About the Circumference of the Cone Model at the Base, M = 2, α = 4°, Re_{ℓ} = 6.10 x 10^6

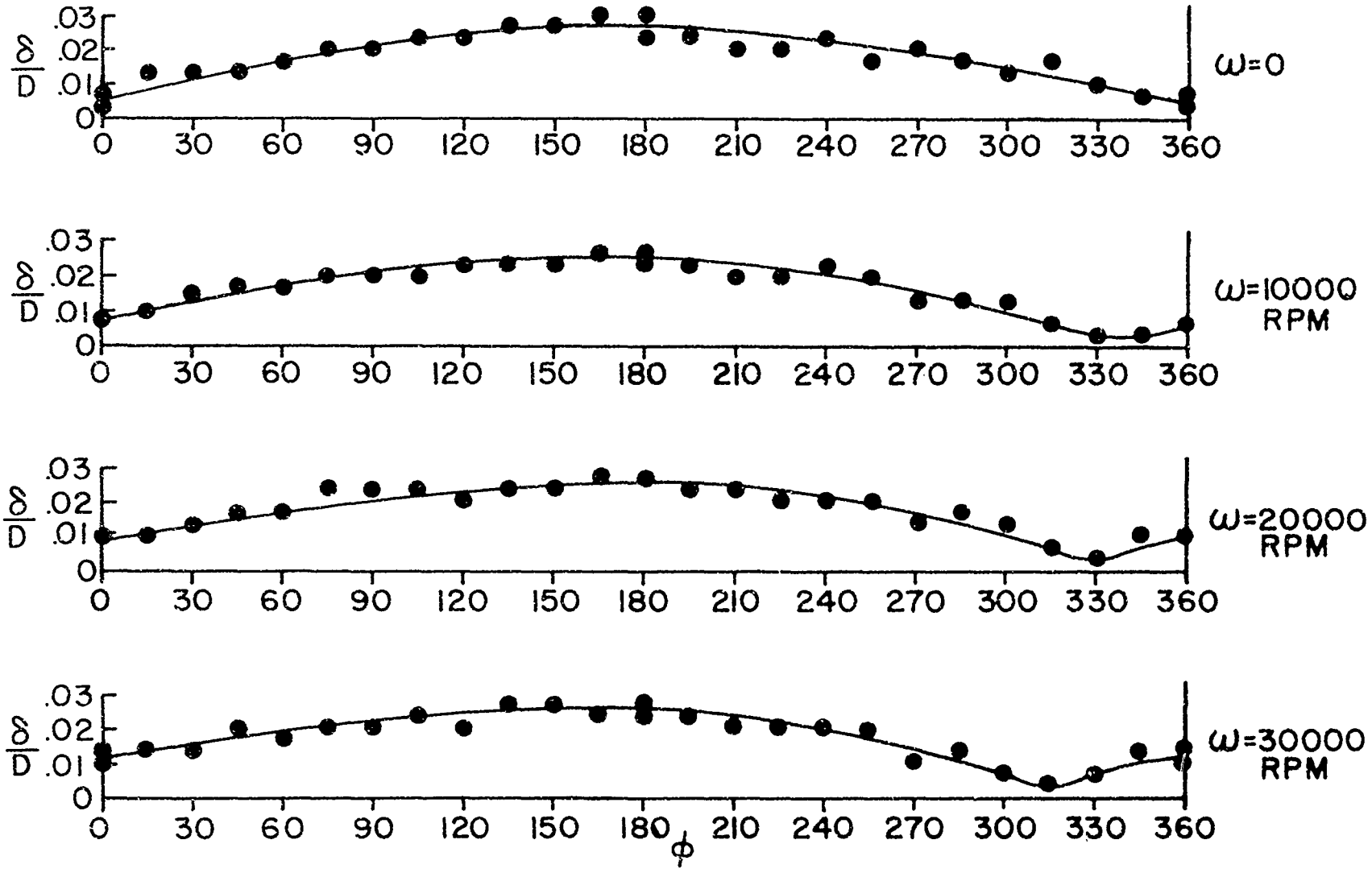

Figure 9D. Distribution of Boundary Layer Thickness About the Circumference of the Cone Model at the Base, M = 3, α = 2°, Re_{ℓ} = 4.80 x 10^6

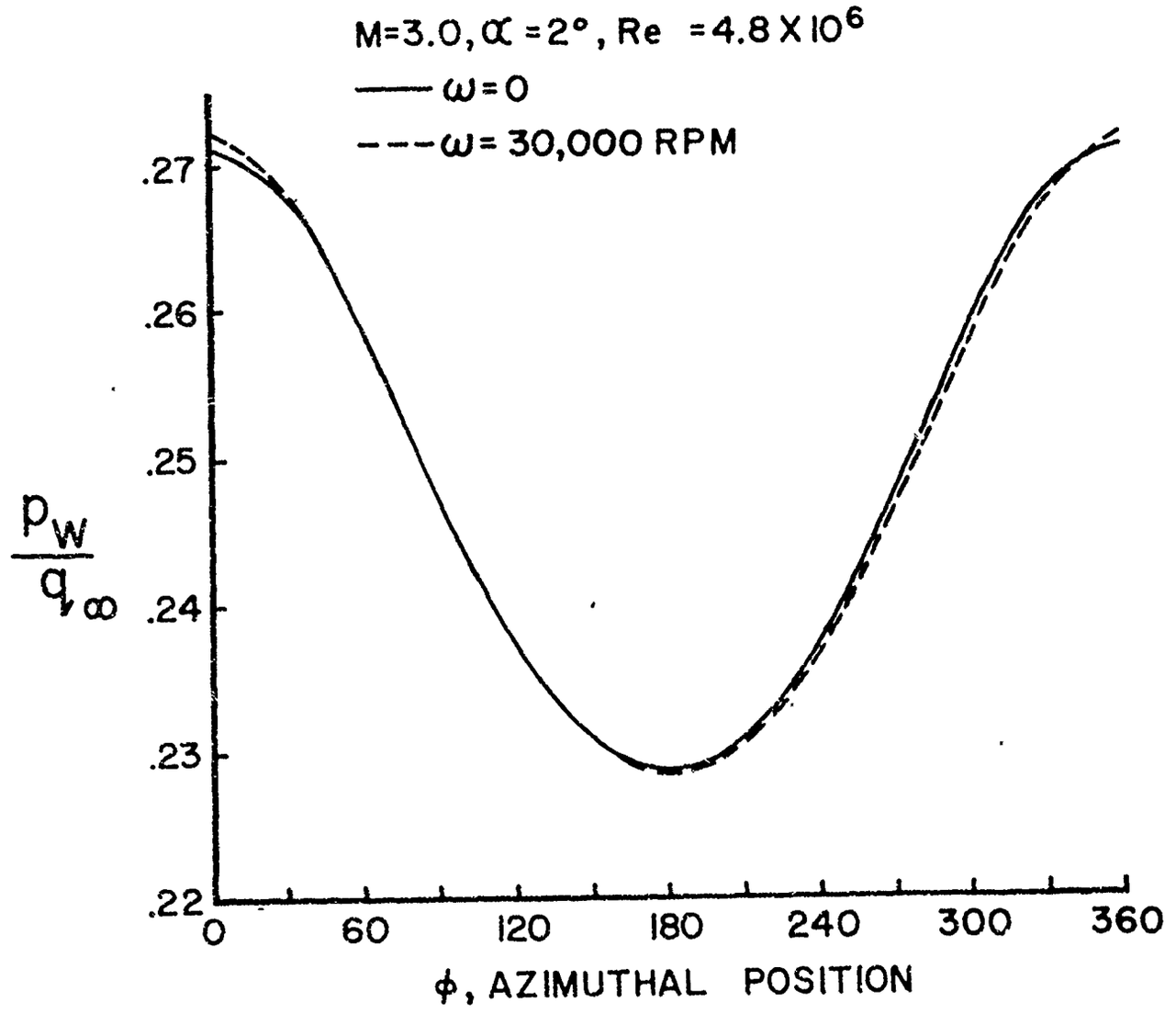

Figure 10. Azimuthal Pressure Distribution About 10° Cone Including Correction for Boundary Layer Displacement

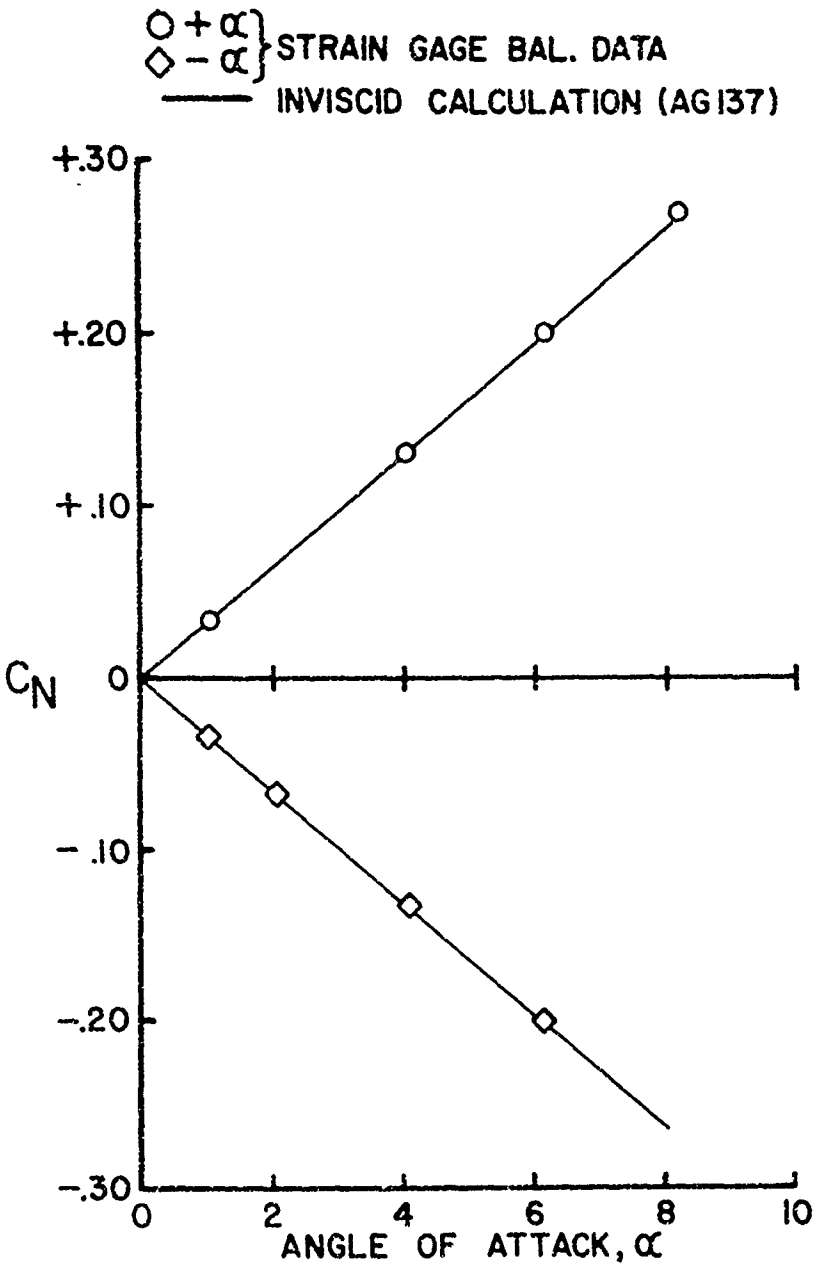

Figure 11. Normal Force Coefficient Vs. Angle of Attack for Cone Model, M = 2, $Re_{\ell} = 6 \times 10^6$

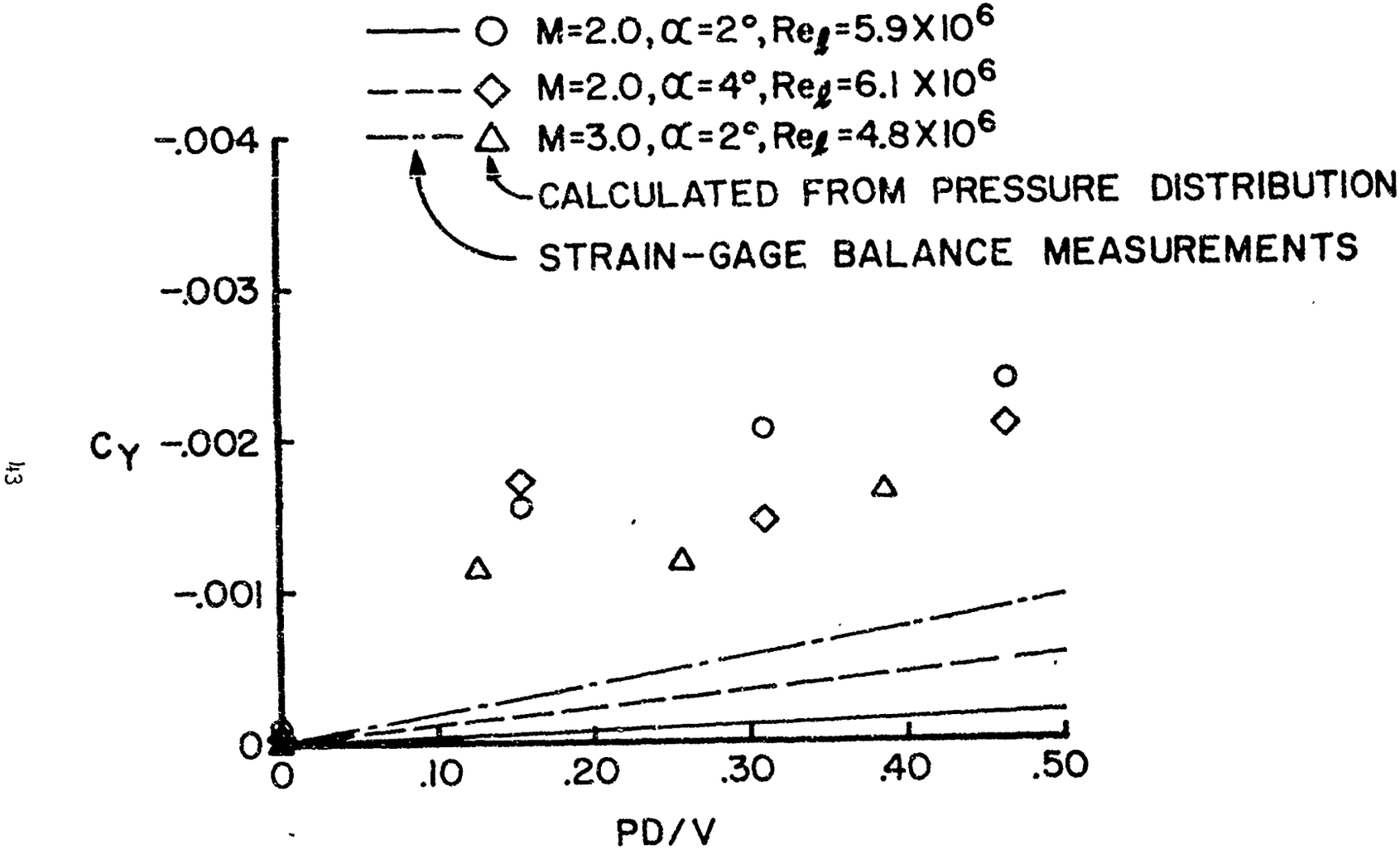

Figure 12. Magnus Coefficient Vs. Spin Rate--Strain Gage Balance Measurements Compared to Coefficients Calculated from the Wall Pressure Distribution

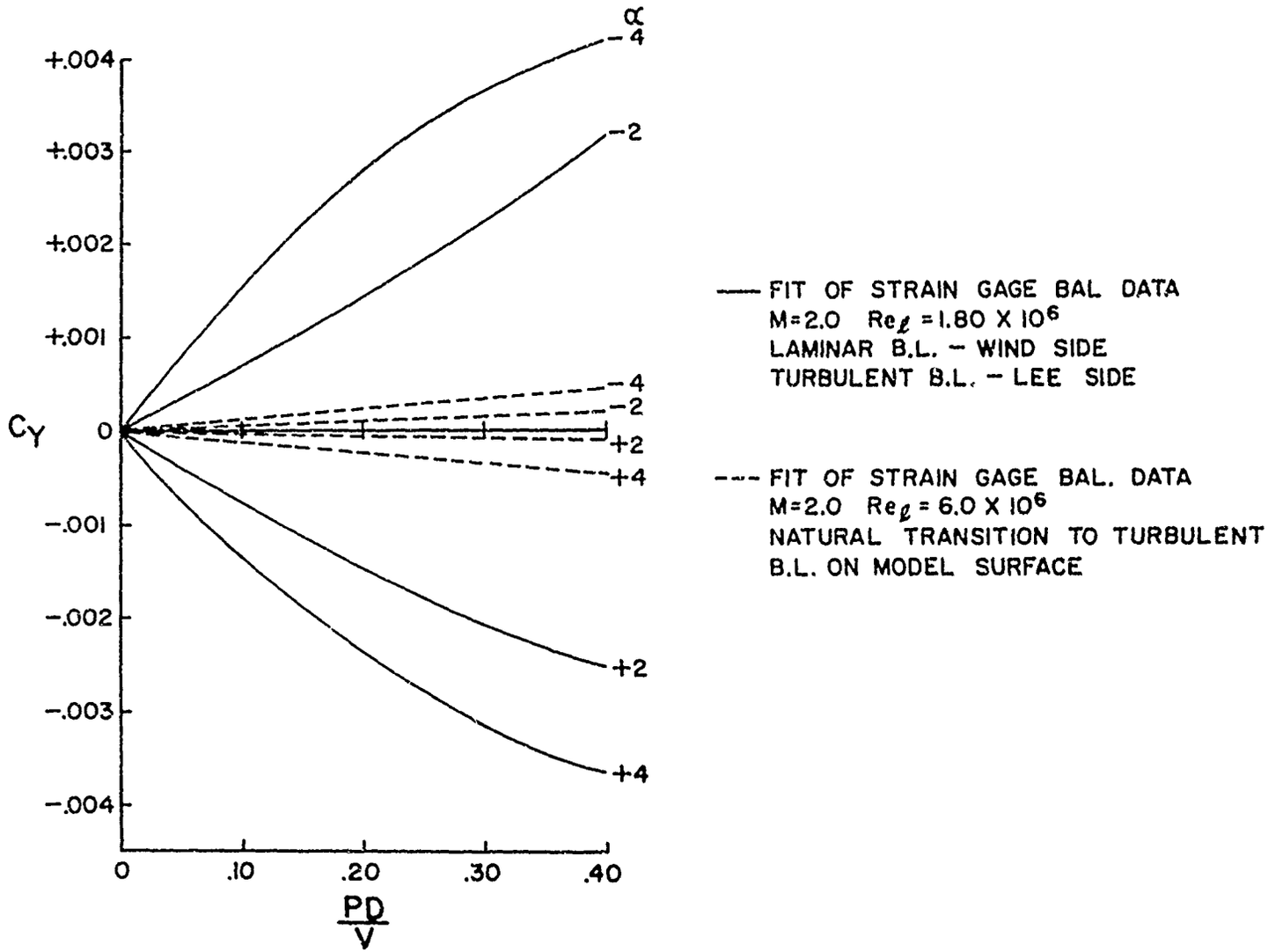

Figure 13. Magnus Coefficient Vs. Spin Rate for Cone Model Comparing Measurements for Transitional Boundary Layers.

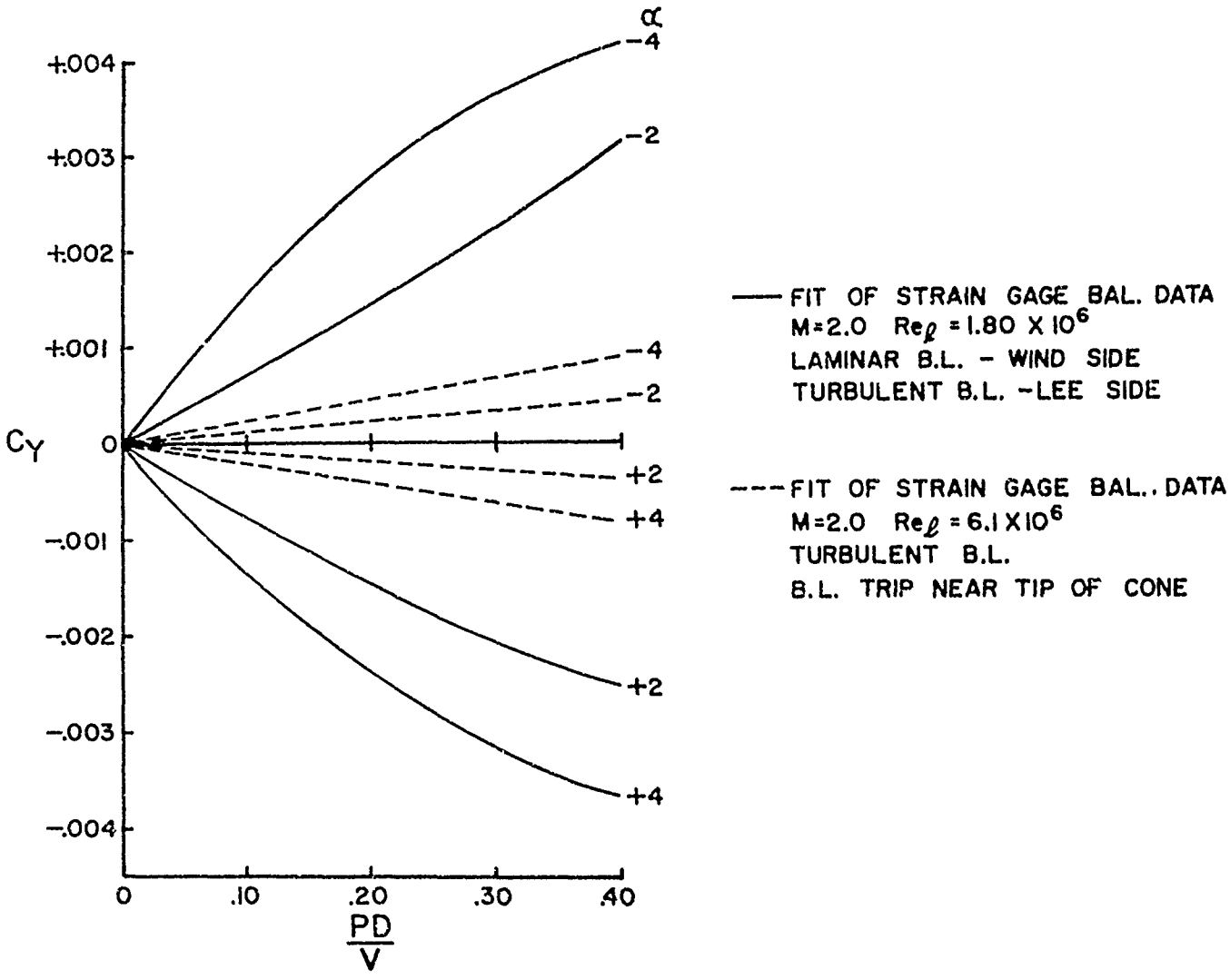

Figure 14. Magnus Coefficient Vs. Spin Rate of Cone Model Comparing Measurements for Transitional and Tripped Turbulent Boundary Layers